CHAPTER TEN
Thermal history

Summary

Subsidence in sedimentary basins causes thermal maturation in the progressively buried sedimentary layers. Indicators of the thermal history include organic, geochemical, mineralogical and thermochronometric measurements. The most important factors in the maturation of organic matter are temperature and time, pressure being relatively unimportant. This temperature and time dependency is described by the *Arrhenius equation*, which states that the reaction rate increases exponentially with temperature; the rate of the increase, however, slows with increasing temperature. The cumulative effect of increasing temperature over time can be evaluated by integrating the reaction rate over time. This is called the *maturation integral*. It can be related directly to measurable indices of burial.

Paleotemperatures are controlled by the basal heat flow history of the basin (which in turn reflects the lithospheric mechanics), but also by 'internal' factors such as variations in thermal conductivities, heat generation from radioactive sources in the continental crust and within the sedimentary basin-fill, effects of sediment deposition rate producing thermal blanketing, regional water flow through aquifers and surface temperature variation. Heat flow heterogeneities may be caused by the presence of salt diapirs and fractures permitting advective heat transport by fluids, and by the heating effects of igneous sills and dykes.

Thermal conductivity models of the basin-fill can be developed from knowledge of framework mineralogy and porosity. The effect of a heterogeneous basin-fill, assuming a constant heat flow, is an irregular rather than linear geotherm, particularly where there is a wide range of insulating (for example marine shale) and conducting (for example salt) lithologies. Radiogenic heat production is greatest where the underlying basement is granitic, and where the basin-fill contains 'hot' shales. Radiogenic heat production is particularly important in deep, long-lived basins. Advection of fluids along regional aquifers has profound consequences for heat flow in basins and can locally override basal heat flow contributions. Advective heat transport depends on the temperature of the pore fluids, but also on rock porosity. Although compactionally driven fluid movement is slow and thermally relatively ineffective, gravitationally driven flow through aquifers is very important. Recharge areas of water in topographically elevated areas around the basin margin, such as in foreland basins, rifts and intracratonic sags, displaces basinal brines and strongly affects the temperature history of basin sediments. Major climatic changes of long frequency cause temperature changes to be propagated through the upper part of the basin-fill that may affect thermal indicators.

Subsurface temperatures can be estimated from borehole measurements, with a correction applied to account for the cooling that takes place during the circulation of drilling fluids. These corrected formation temperatures allow near-surface geothermal gradients to be calculated.

Vitrinite reflectance is the most widely used organic indicator of thermal maturity. Other organic and mineralogical indicators are also used. Apatite fission track analysis is now a well-established thermochronological tool, and the diffusion of helium during U–Th decay is an increasingly used technique. Both thermochronometers allow the timing of thermal events as well as the maximum paleotemperature to be assessed.

Vitrinite reflectance measurements plotted against depth – termed R_o profiles – provide useful information on the thermal history of the basin. The 'normal' pattern is a sublinear relationship between log R_o and depth, indicating a continuous, time-invariant geothermal gradient. R_o profiles with distinct kinks between two linear segments (doglegs) indicate two periods of different geothermal gradient separated by a thermal event. R_o profiles with a sharp break or jump (offsets) indicate the existence of an unconformity with a large stratigraphic gap. The R_o profile in basins that have undergone continuous subsidence intersect the surface at values of 0.2 to 0.4% R_o. Inverted basins that have lost the upper part of the basin-fill by crustal uplift and erosion have profiles intersecting the surface at higher values of R_o. The offset of the R_o profile from the 'normal' profile can be used to estimate the amount of denudation, but care needs to be taken with the possible effects of thermal conductivity variations in the basin and the correct choice of surface temperature at the time of maximum paleotemperature of the basin-fill.

Burial of thermochronometers in sedimentary basins, such as apatite fission track and U–Th/He, may cause partial or full annealing. Quartz cementation is also temperature-dependent, taking place at 90–120 °C, and typically at depths of 2500–4500 m. Quartz cementation arrests further mechanical compaction.

Studies of present-day heat flows and ancient geothermal gradients suggest that thermal regime closely reflects tectonic history. In particular, *hypothermal* (cooler than average) basins include ocean trenches and outer forearcs and foreland basins. *Hyperthermal* (hotter than average) basins include oceanic and continental rifts, some strike-slip basins with mantle involvement, and magmatic arcs in collisional settings. Mature passive margins that are old compared to the thermal time constant of the lithosphere tend to have near-average heat flows and geothermal gradients.

Basin Analysis: Principles and Application to Petroleum Play Assessment, Third Edition. Philip A. Allen and John R. Allen.

10.1 Introduction

Subsidence in sedimentary basins causes material initially deposited at low temperatures and pressures to be subjected to higher temperatures and pressures. Sediments may pass through diagenetic, then metamorphic regimes and may contain indices of their new pressure-temperature conditions. Thermal indices are generally obtained from either dispersed organic matter, temperature-dependent chronometers such as fission tracks in apatite and zircon or from mineralogical trends. A great deal of effort has been spent in attempting to find an analytical technique capable of unambiguously describing thermal maturity, and an equal amount of effort attempting to correlate the resulting proliferation of indicators.

Numerical values of the organic geochemical parameters are dependent on time, thermal energy and type of organic matter (e.g. Weber & Maximov 1976 for an early contribution). The evolution of clays and other minerals is controlled by temperature and by chemical and petrological properties. The scale of maturation to which a given organic or mineralogical phase can be calibrated is that of *coal rank*. Any analytical technique must be able to make use of very small amounts of dispersed organic matter in order to be valuable in basin analysis. Vitrinite reflectance and elemental analyses enable coal rank to be related to hydrocarbon generation stages. Thermochronological tools such as apatite fission track analysis and the diffusion of He during U–Th decay offer the important advantage of providing information on thermal evolution instead of solely on maximum paleotemperature reached.

The objective in this chapter is to describe the use of a number of thermal indicators in constraining and calibrating the thermal evolution of the basin-fill. The implications for the generation of hydrocarbons and for the diagenesis of reservoir rocks are developed in Chapter 11. Fundamentals on heat flow are given in §2.2.

10.2 Theory: the Arrhenius equation and maturation indices

It is now believed that the effects of depth *per se* on the maturation of organic matter are of minor importance, the most important factors being *temperature* and *time*. Pressure is relatively unimportant. Philippi (1965) assessed the effect of pressure by studying hydrocarbons in two Californian basins. In the Los Angeles Basin, hydrocarbons were generated at about 8,000 ft (~2.4 km) whereas in the Ventura basin, generation did not take place until about 12,500 ft (3.8 km) of burial. Since pressure or stress is directly related to depth of burial ($\sigma = \rho gh$) this suggests that pressure does not play a major role in hydrocarbon generation. However, the generation of hydrocarbons in the two basins took place at the same temperature, strongly suggesting that subsurface temperature was the overriding control.

The relationship between temperature and the rate of chemical reactions is given by the *Arrhenius equation*:

$$K = A\exp(-E_a/RT) \qquad [10.1]$$

where K is the reaction rate, A is a constant sometimes termed the *frequency factor* (it is the maximum value that can be reached by K when given an infinite temperature), E_a is the activation energy, R is the universal gas constant, and T is the absolute temperature in kelvin. The constants in the Arrhenius equation can be estimated from compilations of organic metamorphism (e.g. Hood *et al.* 1975; Shibaoka & Bennett 1977). The activation energies of each individual reaction involved in organic maturation are not known, but for each organic matter type a distribution of activation energies may be established from laboratory and field studies. For example, a distribution of activation energies for the maturation of vitrinite from 159 to 310 kJ mol^{-1}, centred on 226 kJ mol^{-1}, was suggested by Burnham and Sweeney (1989).

The Arrhenius equation suggests that reaction rates should increase exponentially with temperature, so that a 10 °C rise in temperature causes the reaction rate to double. This result is widely known, but it is less widely realised that the rate of increase in reaction rate slows down with increasing temperature, so at 200 °C the reaction rate increases by a factor of 1.4 for a 10 °C rise in temperature (Robert 1988). Clearly, both time and temperature influence organic maturation, a view supported by the occurrence of shallower oil generation thresholds as the sediments containing the organic matter become older (Dow 1977). Connan (1974) believed that the threshold of the principal zone of oil generation was related to the logarithm of the age of the formation, further supporting a time-temperature dependence obeying the laws of chemical kinetics.

The cumulative effect of increasing temperature can be evaluated from the *maturation integral*, the reaction rate integrated over time,

$$C = A\int_0^t \exp(-E_a/RT) + C_0 \qquad [10.2]$$

where C_o is the original level of maturation of the organic material at the time of deposition ($t = 0$). The maturation integral for any nominated horizon can be calculated if the decompacted burial history (Chapter 9), heat flow through time, and thermal conductivities of the sediments and basement are known or can be assumed. For the less mathematically inclined, eqn. [10.2] shows that when paleotemperatures are plotted on an exponential scale, the area under the curve from deposition to a given time is proportional to the maturation integral at that time at the nominated horizon (plus the value of C_0). Some authors believe that the maturation integral is related to measurable values of vitrinite reflectance (see §10.4.2) (Royden *et al.* 1980; Falvey & Middleton 1981).

Hood *et al.* (1975) devised an artificial maturation parameter, the *level of organic metamorphism* (LOM), based on a rank progression of coals, from lignites to meta-anthracites. Hood's diagram shows the relationship between the 'effective heating time' and the maximum temperature attained. The effective heating time is defined as the length of time the temperature remains within a 15 °C range of the maximum temperature. This method, although not stated explicitly by Hood *et al.* (1975), is based on the first-order chemical kinetics outlined above.

Another application of the Arrhenius relationship is the *time-temperature index* (TTI) (Lopatin 1971; Waples 1980). This index is based on the view that the reaction rate doubles for every 10 °C rise in temperature over the entire range from 50 °C to 250 °C. Since the method assumes that the reaction rate continues to double in 10 °C intervals over the entire temperature range to 250 °C, it tends to overestimate maturity. The reaction cannot continue indefinitely because the materials undergoing thermal maturation are used up.

Other techniques, such as those of Tissot (1969), Tissot and Espitalié (1975) and Mackenzie and Quigley (1988), have been developed that enable masses of petroleum generated during thermal matura-

tion of organic matter to be calculated. The Mackenzie and Quigley model is described in relation to petroleum source rocks in §11.4.

10.3 Factors influencing temperatures and paleotemperatures in sedimentary basins

Chapter 2 contains some basic concepts about heat flow, and the specific problem of one-dimensional (vertical) heat flow in basins due to stretching is addressed in Chapter 3. Here, we are concerned with the various 'internal' factors that influence the temperatures within sedimentary basins: (i) variations in thermal conductivity, most commonly due to lithological heterogeneity; (ii) internal heat generation; (iii) convective/advective heat transfer within fractured and unfractured sediments; and (iv) surface temperature changes.

10.3.1 Effects of thermal conductivity

The distribution of temperature with depth (geotherm) in the continents is primarily determined by conductive heat transport. We know the relation between heat flux and temperature gradient, as given by Fourier's law (eqn. 2.29). This law states that conductive heat flux is related to the temperature gradient by a coefficient, K, known as the coefficient of *thermal conductivity*. If two measurements of temperature are known, one T_y at depth y and another T_0 at the surface ($y = 0$), Fourier's law can be restated as

$$q = -K(T_y - T_0)y \qquad [10.3]$$

which by rearrangement becomes

$$T_y = T_0 + \left(\frac{-qy}{K}\right) \qquad [10.4]$$

where q is the heat flux (negative for y increasing downwards). We are here initially ignoring internal heat production within the sedimentary pile.

Ignoring also for the moment lithological variations, thermal conductivities of sediments vary as a function of depth because of their porosity loss with burial (§9.3). Eqn. [10.4] can be modified to account for the different thermal conductivities of the sedimentary layers,

$$T_y = T_0 + (-q)\left\{\frac{l_1}{K_1} + \frac{l_2}{K_2} + \frac{l_3}{K_3} + \cdots\right\} \qquad [10.5]$$

where l_1 to l_n are the thicknesses of the layers with thermal conductivities K_1 to K_n, and $l_1 + l_2 + l_3 \ldots$ must of course be equal to y. Falvey and Middleton (1981) recommended the use of a function that assumed an exponential relation between porosity and depth

$$K = K_{min} - \{(K_{min} - K_0)\exp(-\gamma y)\} \qquad [10.6]$$

where K_{min} is the thermal conductivity deep in the sedimentary section, K_0 that at the sediment surface, and γ is a constant for a given section. Since K varies with depth, temperature gradients must also vary with depth in order to maintain a constant heat flow. If present-day heat flow can be calculated from a borehole by measurement of conductivities and surface and bottom hole temperatures, eqns [10.4] and [10.6] can be used to find the temperature at any depth. If paleoheat flow is then assumed to be constant with depth, the temperature history of any chosen stratigraphic level can be estimated. The assumption of a constant heat flow with depth is a condition of any one-dimensional steady-state heat conduction model. Measurements in some sedimentary basins such as the North Sea failed rift (Andrews-Speed *et al.* 1984), however, suggest that this is not a good assumption, deep circulation of water most likely being responsible for the departure from the steady-state assumption (see §10.3.4).

A fundamental requirement in the estimation of geotherms, temperatures and paleotemperatures in sedimentary basins is therefore the bulk thermal conductivity of the different sedimentary layers making up the basin-fill. Thermal conductivities can be measured in the laboratory (Carslaw & Jaeger 1959; Sass *et al.* 1971) and *in situ* (Beck *et al.* 1971). The bulk thermal conductivity of most sedimentary rocks ranges between 1.5 $Wm^{-1}K^{-1}$ (shales) and 4.5 $Wm^{-1}K^{-1}$ (sandstones) (Table 10.1). These estimates depend mostly on the mineralogy of the framework grains, the type and amount of material in the matrix (commonly clay minerals), and the porosity and fluid content (commonly water) (Brigaud & Vasseur 1989). The individual conductivities of framework, matrix and pore fluid are also dependent on temperature. The general trend is that non-argillaceous rocks have higher conductivities than argillaceous rocks, and that conductivity increases with increasing porosity. If measurements of the thermal conductivities of the different components in a rock can

Table 10.1 Density and thermal properties of some common minerals and rock types. Thermal conductivities are given at surface temperatures (in part from Brigaud and Vasseur 1989).

Rock type	Density (kg m^{-3})	Thermal conductivity K ($Wm^{-1}K^{-1}$)	Volumetric coefficient of thermal expansion α_v ($10^{-5}K^{-1}$)
Minerals common in sediments and sedimentary rocks			
Water (pore fluid)	1000	0.6	
Quartz	2650	7.7	
Calcite	2710	3.3	
Dolomite	2870	5.3	
Anhydrite	2960	6.3	
Kaolinite	2630	2.6	
Chlorite	2780	3.3	
Illite/smectite	2660	1.9	
Sedimentary rocks			
Shale	2100–2700	1.2–3.0	
Sandstone	1900–2500	1.5–4.2	3
Limestone	1600–2700	2.0–3.4	2.4
Dolomite	2700–2850	3.2–3.5	
Metamorphic rocks			
Gneiss	2600–2850	2.1–4.2	
Amphibolite	2800–3150	2.1–3.8	
Igneous rocks			
Basalt	2950	1.3–2.9	
Granite	2650	2.4–3.8	2.4
Gabbro	2950	1.9–4.0	1.6
Peridotite	3250	3.0–4.5	2.4

be made, the bulk thermal conductivity of the sedimentary layer can be estimated. The overall thermal conductivity structure of the basin-fill can then be estimated from a knowledge of the mineralogy, porosity and fluid content of the stratigraphy filling the basin. The availability of large 'continuous' subsurface data sets from hydrocarbon exploration boreholes has revolutionised the ability to make such estimates.

The *effective thermal conductivity* of a clean quartzose sandstone with pore-filling water should decrease with increasing porosity, since the pore fluid is insulating. However, the effective thermal conductivity of a clean quartzose sandstone may be almost invariant with depth (Fig. 10.1b). This is due to the decrease in conductivity of the framework quartz grains with increasing temperature, which offsets the increase in conductivity due to compaction (porosity loss) (Palciauskas 1986).

The effects of clays in a sandstone, for example as pore-filling authigenic cements, is to decrease the bulk thermal conductivity of the argillaceous sandstone, since clays have an insulating effect (Fig. 10.1a). Feldspar and most clays do not show a marked effect of temperature on thermal conductivity, so the effect of compaction commonly dominates. A clay-water mixture (shales) increases in conductivity rapidly with depth because of compaction, whereas a feldspar-water mixture, because it compacts similarly to a sand, increases in conductivity much more slowly with depth (Fig. 10.1c).

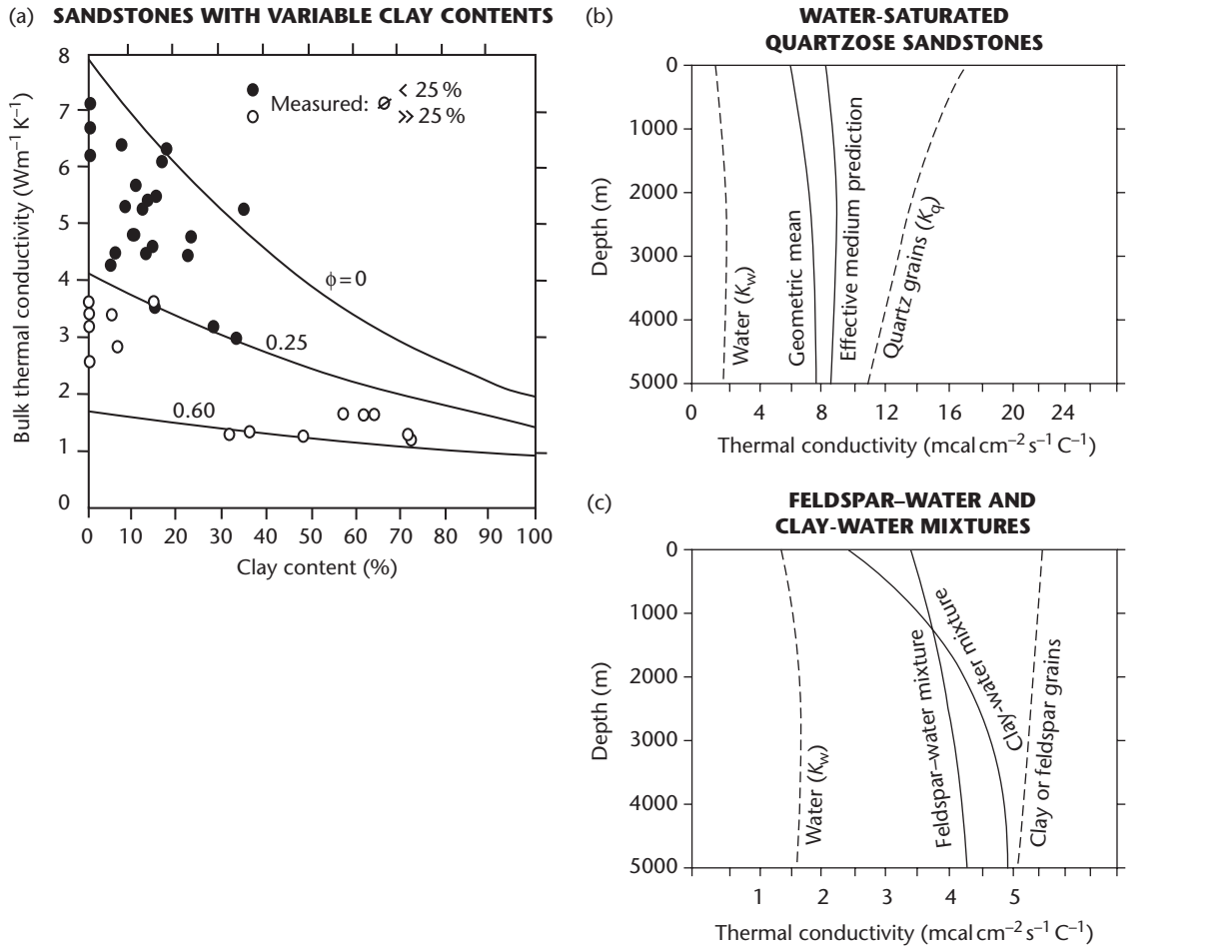

Fig. 10.1 The thermal conductivities of sedimentary rocks. (a) Influence of mineralogy on thermal conductivity of water-saturated sandstones with a variable clay content, using thermal conductivities of $7.7\,W\,m^{-1}\,K^{-1}$, $2.0\,W\,m^{-1}\,K^{-1}$ and $0.6\,W\,m^{-1}\,K^{-1}$ for quartz, clay and water respectively (after Brigaud & Vasseur 1989, reproduced with permission of John Wiley & Sons, Ltd.). (b) Thermal conductivity of water-saturated quartzose sandstone as a function of depth. The effective medium prediction and the empirical relation closely agree, demonstrating a negligible increase in thermal conductivity with depth, despite the fact that the quartz grains decrease in thermal conductivity considerably with depth. (c) Feldspar-water and clay-water mixtures, showing that the thermal conductivities increase markedly with depth, especially for clay-rich sediments. This is principally due to the effects of compaction. In (b) and (c) the temperature gradient is $30\,°C\,km^{-1}$ and the surface temperature 20 °C. After Palciauskas (1986), reproduced with permission from Editions Technip.

The bulk conductivity of a sediment layer can therefore be thought of as being made up of the contributions of the pore fluid and the grain conductivities. Assuming a geometric mean model for the two-phase media of solid and fluid (Woodside & Messmer 1961), the bulk conductivity is

$$K_{bulk} = K_s^{(1-\phi)} K_w^{\phi} \qquad [10.7]$$

where K_s and K_w are the thermal conductivities of sediment grains and water respectively, and ϕ is the porosity, assumed to be filled with water. An alternative method, termed the *effective medium* theory calculates an effective bulk thermal conductivity for a randomly inhomogeneous medium made of constituents with volume fractions V_i and thermal conductivities K_i. The basic result of the theory is

$$K^{-1} = \sum_{i=1}^{n} 3V_i(2K + K_i)^{-1} \qquad [10.8]$$

This expression is particularly useful where mixed components are present in the sediment layer. For example, for the water-quartz mixture mentioned above, if the quartz framework (K_q = 5.4 W m^{-1} °C^{-1} at T = 100 °C) occupies 0.7 of the rock volume, and water (K_w = 0.7 W m^{-1} °C^{-1} at T = 100 °C) occupies 0.3 of the rock volume, the bulk conductivity from effective medium theory (eqn. [10.8]) is approximately 3.3 W m^{-1} °C^{-1}. From the general result in eqn. [10.7], the bulk conductivity is approximately 2.9 W m^{-1} °C^{-1}.

A fundamental result of maintaining a constant heat flux through a heterogeneous basin-fill is that the geothermal gradient must vary with depth. As an example, consider the thermal conductivity structure derived from the borehole shown in Fig. 10.2a. Keeping the heat flux at 63 mW m^{-2}, the geotherm varies as in Fig. 10.2b. Clearly, the presence of a heterogeneous basin-fill negates the assumption of a linear conduction geotherm. The implications for the interpretation of maturity profiles are discussed in §10.5.

10.3.2 Effects of internal heat generation in sediments

Heat generation by radioactive decay in sediments may significantly affect the heat flow in sedimentary basins (Rybach 1986). Although all naturally occurring radioactive isotopes generate heat, the only significant contributions come from the decay series of uranium and thorium and from ^{40}K (Table 10.2). As a result, heat production varies with lithology, generally being lowest in evaporites and carbonates, low to medium in sandstones, higher in shales and siltstones and very high in black shales (Rybach 1986; Haack 1982; Rybach & Cermak 1982).

In the continents, crustal radioactivity may account for a large proportion (20–60%) of the surface heat flow (§2.2.3). For a purely conductive, one-dimensional (vertical) heat flow, the temperature at any depth y is determined by the surface temperature T_0, the basal heat flow q_b, the average thermal conductivity of the sediments K, and the internal heat production A (estimated from natural gamma ray logs). The effect of the internal heat generation is greatest at large depths, as can be seen from the third term in eqn. [2.26] (Fig. 10.3). The temperature increase after a time t as a result of the internal heat generation depends on the value of A, but the net temperature change also depends on the rate of conductive heat loss. Over geological time scales of >10 Myr the temperature rise may be considerable

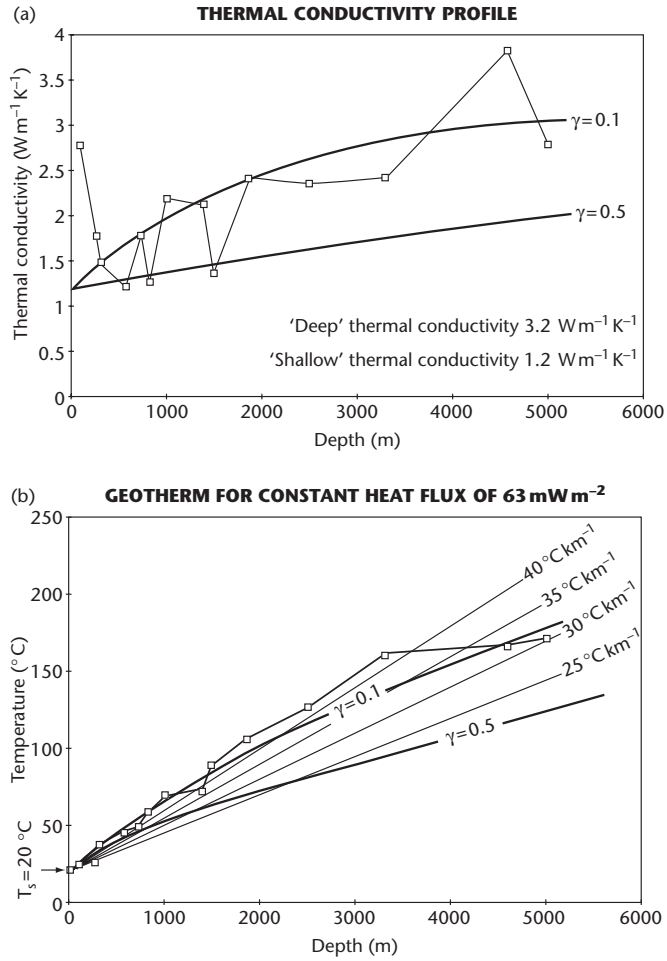

Fig. 10.2 (a) Thermal conductivity structure of stratigraphy penetrated by borehole 14/20-1 close to Wexford, southeastern Ireland. Two curves represent exponential distribution of thermal conductivity with depth with a depth constant γ of 0.1 and 0.5. The thermal conductivity in the deep section is c.3.2 W m^{-1} K^{-1}, and c.1.2 W m^{-1} K^{-1} in the shallow, near-surface section (see eqn. [10.6]). (b) Geotherm using the thermal conductivity structure in (a) for the borehole 14/20-1, exponential distributions of thermal conductivity with γ of 0.1 and 0.5, and a constant basal heat flow of 63 mW m^{-2}. Linear geotherms between 25 and 40 °C km^{-1} are shown for comparison.

Table 10.2 Typical concentrations of heat-producing elements in various rock types

Rock type	U (ppm)	Th (ppm)	K (%)
Granite	4.7	20	4.2
Shale	3.7	12.0	2.7
Average continental crust	1.42	3.6	1.43
Reference mantle	0.031	0.124	0.031
Chondritic meteorite	0.008	0.029	0.056

(Rybach 1986, p. 317). Internal heat generation in sediments may therefore strongly affect the temperature field in the basin if it is deep (>5 km) or long lived (>10 Myr).

10.3.3 Effects of sedimentation rate and sediment blanketing

The presence of a thick cover of sedimentary rocks with high radiogenic heat production has the effect of 'blanketing' the underlying crust and deeper parts of the sedimentary basin (Karner 1991; Wangen 1995, 2010 p. 181). This blanketing effect may be important in terms of the temperature-dependent rheology of rocks underlying the basin, but more importantly in the present context in elevating paleotemperatures in the basin-fill.

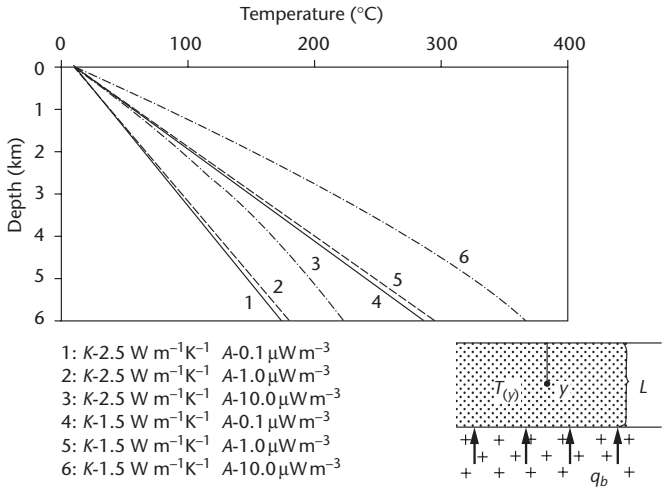

Fig. 10.3 The influence of internal heat generation per unit volume in the sedimentary column A and thermal conductivity K on the distribution of temperature with depth $T(y)$. The different curves were calculated by Rybach (1986) for a thickness of the heat-producing zone of 6 km, a basal heat flux q_b of 70 mW m^{-2} and a surface temperature T_0 of 20 °C. Reproduced with permission from Editions Technip.

The effect of sediment blanketing is described in §2.2.4. As a reminder, the deposition of sediments has two effects, first a transient cooling and reduction in the surface heat flow, and, second, a possible long-term warming, dependent on the thermal conductivity and internal heat generation of the new sediment layer, or blanket. The effectiveness of the sediment blanket in causing a temperature transient depends on two main factors: (i) the deposition rate; and (ii) the thermal conductivity of the young sediments comprising the blanket.

A fast deposition rate causes the underlying sediment column to be covered with cool sediments deposited at surface temperatures. During burial, these new sediments do not heat up rapidly enough to offset the cooling effect on the geotherm. This thermal response time is greatest for *instantaneous* deposition and may be >1 Myr for the instantaneous deposition of 1 km of sediment. A deposition rate of >0.1 mm yr^{-1} is required to depart from a stationary state for the geotherm. Rapid deposition of, for example, 1 km of sediments in just 0.1 Myr would reduce the surface heat flow by half. The transient temperature field may extend several kilometres into the basin-fill (see §10.3.5 for discussion of 'skin depth'). This effect of blanketing may be especially relevant in the thick sedimentary successions deposited at the mouths of major river deltas.

The temperature transient is also amplified by the deposition of low thermal conductivity, uncompacted sediments with large volumes of saline pore water (K_w = 0.6 W m^{-1} K^{-1}). Consequently, the sediment blanket retards the rapid heating of the newly deposited sediments. Highly porous, uncompacted marine shales, such as may be deposited offshore from suspended load-dominated rivers, may therefore act as strong insulators in this way.

Fig. 10.4 shows the effects of sedimentation rate and thermal conductivity of the sediment blanket on the geotherm and surface heat flow. The solution is given in Appendix 12.

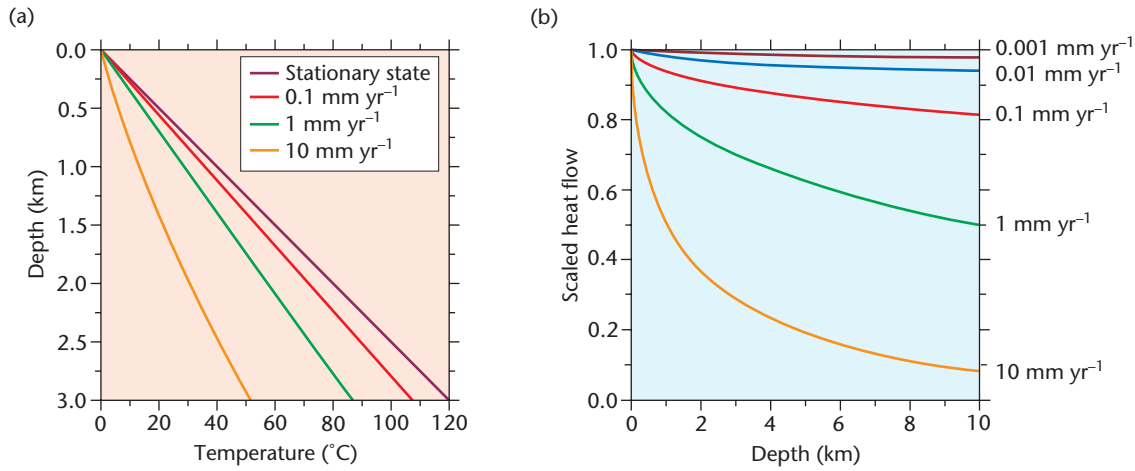

Fig. 10.4 Effect of a sediment blanket for a range of deposition rates. (a) Geotherms in the basin-fill for deposition rates of 0.1, 1 and 10 mm yr^{-1}, at the time when 3 km of sediment has been deposited (30 Myr, 3 Myr and 0.3 Myr respectively), including the steady-state conduction geotherm prior to sedimentation (stationary state). (b) Surface heat flux scaled against the surface heat flow before the onset of sedimentation for a range of deposition rates from 0.001 mm yr^{-1} to 10 mm yr^{-1}, as a function of the thickness of basin sediments. Basin thickness is the product of the sedimentation velocity and time. After Wangen (2010, fig. 6.38). © Magnus Wangen 2010, reproduced with the permission of Cambridge University Press.

10.3.4 Effects of advective heat transport by fluids

The temperatures in sedimentary basins may also be affected by the advective flow of heat through regional aquifers. Such processes may cause anomalously low surface heat flows at regions of recharge, and anomalously high surface heat flows in regions of discharge. The heat flow distributions of the Great Plains, USA (Gosnold & Fischer 1986), and the Alberta Basin (Majorowicz & Jessop 1981; Majorowicz *et al*. 1984) have been explained in this way.

It is important to know the relative contributions of conduction from the interior of the Earth, internal heat production from radiogenic decay (and chemical reactions), and advective transport of fluids through pore space. We perform this heat balance in Appendix 7 and, taking reasonable parameter values for a deeply buried rock in a sedimentary basin, calculate the role of advection in controlling the heat flow (see Appendix 59). Compactionally driven flow is too slow to cause significant thermal effects in a basin, whereas the relatively fast pore water flow velocities associated with groundwater movement in regional aquifers may lead to important heating or cooling.

The likely impact of fluids on the thermal history of the basin-fill is linked to the tectonic evolution of the basin. For example, uplift of rift shoulders during stretching of the continental lithosphere may cause meteoric-derived groundwater flows driven by the topographic elevation of the basin flanks. The meteoric fluxes in this case must displace brines filling pore space within the basin-fill. If the density of pore-filling brine is 1028 kg m^{-3} and the density of meteoric water is 1000 kg m^{-2}, a simple pressure balance indicates that the extent of downward penetration of meteoric water is nearly 40 times the topographic elevation of its influx (Bjorlykke 1983). This implies that for even low topographic basin margin uplifts, meteoric gravitationally driven water is able to displace basinal brines from the entire depth of the sedimentary basin. At the other extreme, fluid movement caused by progressive compaction of basin sediments is slow, with vertical rates of <10 mm yr^{-1}, with lower values still as the permeability reduces during compaction (Giles 1987) (Fig. 10.5).

The effects of fluid flow on heat flow in regional-scale systems are well illustrated by the Alberta Basin (Smith & Chapman 1983; Luheshi & Jackson 1986). Using a permeability and thermal conductivity structure for the basin, the raised temperatures at discharge points of fluid flow and lowered temperatures at the recharge areas in the fringing hills can be explained (Fig. 10.6). The model results suggest that the temperature distribution is dominated by convection above the Paleozoic succession, while the heat flows within the Precambrian section can be explained simply by conduction. Andrews-Speed *et al.* (1984) similarly found that heat flow measurements strongly suggested a deep-water circulation, possibly controlled by the configuration of faults, in the North Sea failed rift. The implications of detailed studies such as this are that simple one-dimensional conductive heat flow models may be very poor predictors of actual heat flows in some sedimentary basins. The most strongly affected basins are likely to be continental basins with marginal uplifts, such as foreland basins and some intracratonic rifts and sags.

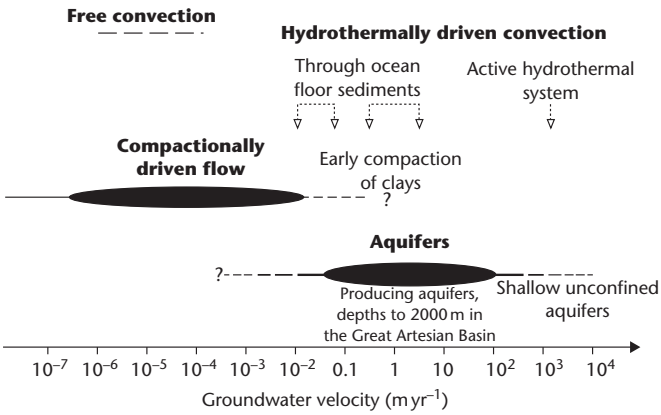

Fig. 10.5 Typical measured pore fluid velocities associated with compactionally driven flow, confined and unconfined aquifers, and hydrothermally driven convection. After Giles (1987, 1997), reproduced with kind permission of Springer Science+Business Media B.V.

10.3.5 Effects of surface temperature changes

The possible effects of surface temperature changes on the maturation of thermal indicators have been relatively neglected, although the effects of, for example, glacial retreat on near-surface temperatures has been evaluated (Beck 1977). The likelihood of a surface temperature change penetrating an underlying basin-fill is essentially a question of heat diffusion (§2.2), and the problem can therefore be approached in a similar way to the cooling of the oceanic lithosphere (§2.2.7). The amount of time necessary for a temperature change to propagate a distance l in a medium with thermal diffusivity κ is

$$t = \frac{l^2}{\kappa} \qquad [10.9]$$

and the characteristic distance (or thermal diffusion distance) over which a temperature change is felt is

$$L = \sqrt{\kappa t} \qquad [10.10]$$

Taking a thermal diffusivity of $\kappa = 10^{-6}$ m^2 s^{-1}, appropriate for the sandstones of a basin-fill, a surface temperature disturbance would be registered at 1 km depth in just over 30 kyr. Expressed differently, the surface temperature change would propagate to a depth of 5.6 km in 1 Myr. We should therefore expect a surface temperature change to rapidly propagate through the upper part of the basin-fill. O'Sullivan and Brown (1998), for example, suggested that the effects of a surface temperature change of c.17 °C during the Miocene on the North Slope of Alaska could be recognised in apatite fission tracks in borehole samples. If geotherms derived from apatite fission track analysis were used to calculate denudation in this example, estimates would be significantly in error.

A key point in this argument is that for thermal indicators to be affected by a surface temperature change, the surface temperature change must be sustained for a prolonged period of time. Yet, climatically induced surface temperature changes tend to be cyclic. What would be the effect of a periodic variation in surface temperature on the geotherm? Temperatures must vary cyclically within a surface zone of the Earth whose thickness is determined by the thermal properties of the crust or basin-fill and the period of the temperature fluctuation. If the temperature variation is described by

$$\omega = \frac{2\pi}{f} \qquad [10.11]$$

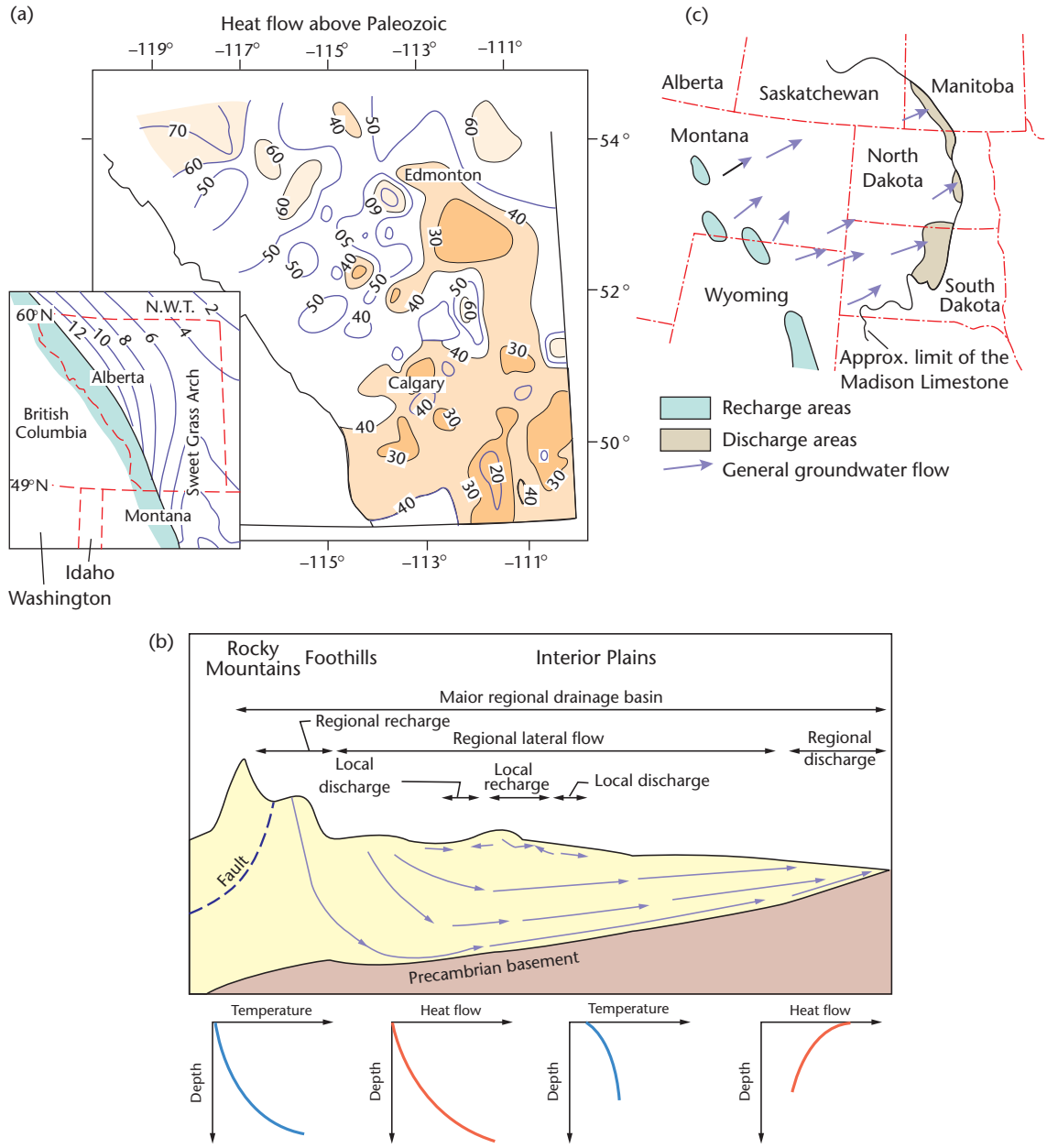

Fig. 10.6 Effects of groundwater flow on surface heat flows in sedimentary basins. (a) Heat flow map of southern and central Alberta, Canada, based on estimated heat flow values (in mW m^{-2}) above the top of the Paleozoic, based on 33,653 bottom hole temperature data from 18,711 wells (Majorowicz *et al*. 1984; reprinted with permission from Elsevier). The heat flows are strongly influenced by groundwater flow from recharge areas in structurally high regions, such as the Sweet Grass Arch (inset), to discharge areas. (b) Pattern of recharge and discharge in a cross-section from the Rocky Mountains to the Great Plains (after Majorowicz *et al*. 1984), and (c) plan view of groundwater flow in the Mississippian (Lower Carboniferous) Madison Limestone aquifer (after Downey 1984).

where f is the period of the temperature variation, we can define a *skin depth* L at which the amplitude of the temperature variation is 1/e of that at the surface of the Earth

$$L = \sqrt{\frac{2\kappa}{\omega}} \qquad [10.12]$$

Using $\kappa = 8 \times 10^{-6}\,m^2\,s^{-1}$, it is clear that the skin depth for daily temperature variations ($\omega = 7.27 \times 10^{-5}\,s^{-1}$) is less than 20 cm, but for Pleistocene climate change variations of frequency 10^5 yr ($\omega = 1.99 \times 10^{-12}\,s^{-1}$), the skin depth is 1 km. This means that long-period variations in surface temperature may be felt deep within the sedimentary basin-fill.

10.3.6 Heat flow around salt domes

Salt structures are found on many passive margins, such as the Gulf of Mexico, West Africa and the Brazilian margin of the South Atlantic

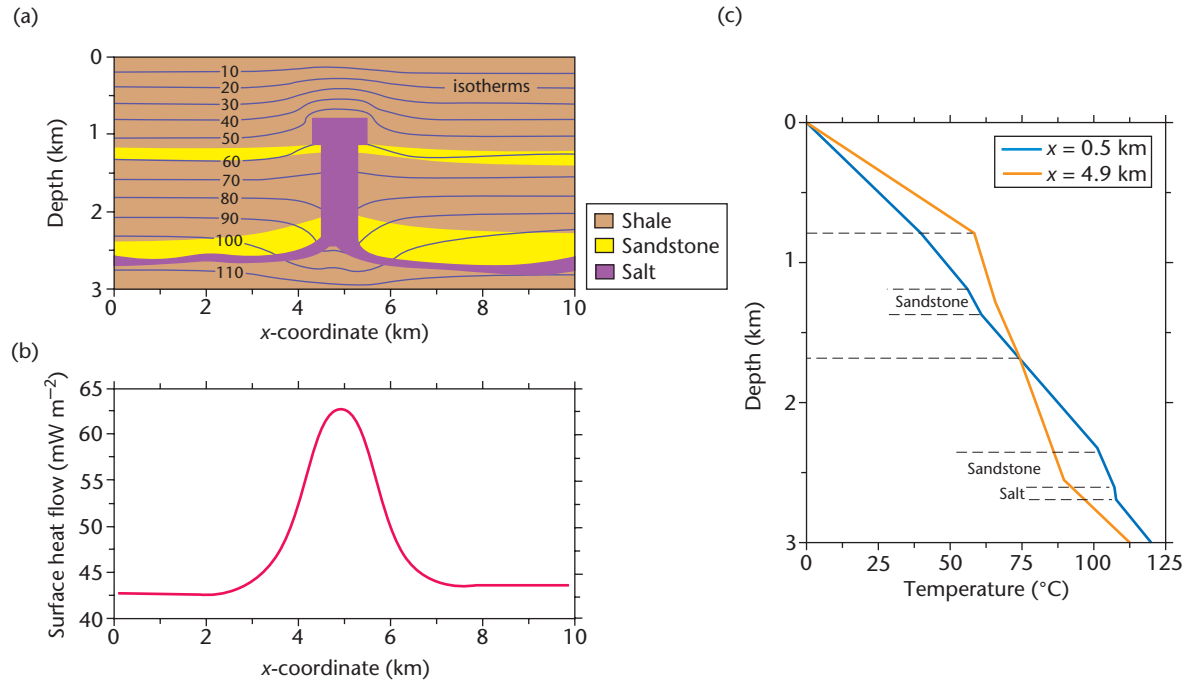

Fig. 10.7 Thermal effects of the presence of a salt diapir in a stratigraphic succession of sandstones and shales. (a) Geometry of salt diapir and isotherms in the subsurface. (b) Surface heat flow (after Wangen 2010, p. 139, fig. 6.15). (c) Geotherms through the centre of the diapir (orange) and to the left side of the model (blue) (after Wangen 2010, fig. 6.16). © Magnus Wangen 2010, reproduced with the permission of Cambridge University Press.

(Hudec & Jackson 2007). Originally deposited as a horizontal sheet, the salt is very mobile because of its rheological weakness, and flows upwards to produce domal diapirs and vertical walls (Gemmer *et al.* 2004). The presence of salt in the subsurface affects heat flow in the sedimentary basin. The reasons for this are straightforward: (i) Salt has a thermal conductivity of ~6 $W\,m^{-1}\,K^{-1}$ at surface conditions and essentially zero porosity, whereas a porous shale has a thermal conductivity of ~1 $W\,m^{-1}\,K^{-1}$; (ii) Salt diapirs cause an extreme three-dimensionality to the temperature field, with hotter conditions above the salt bodies and cooler conditions below, compared with adjacent regions in the enclosing shale. The temperature heterogeneity extends a distance laterally approximately the same as the thickness of the salt diapir (Fig. 10.7). For shallowly buried salt, there is an increase in surface heat flow above the diapir. The increase in surface heat flow scales on the average thermal conductivity from the surface down to a characteristic isotherm. Consequently, if the subscript 1 refers the column to the flank of the diapir, and 2 refers to the vertical column going through the centre of the diapir, the ratio of the surface heat flows scales on the ratio of the thermal conductivities

$$\frac{q_2}{q_1} = \frac{K_1}{K_2} \qquad [10.13]$$

Typical values for the bulk conductivity averaged over depth for the two columns shown in Fig. 10.7 are:

Column 2, comprising salt (4.5 $W\,m^{-1}\,K^{-1}$), shale (1.1 $W\,m^{-1}\,K^{-1}$) and sandstone (2.5 $W\,m^{-1}\,K^{-1}$), has $K_2 = 1.85\,W\,m^{-1}\,K^{-1}$.

Column 1, comprising shale and sandstone, has $K_1 = 1.17\,W\,m^{-1}\,K^{-1}$.

K_2/K_1 is therefore 1.58. This explains the variation in surface heat flow from 42 $mW\,m^{-2}$ on the flank to 63 $mW\,m^{-2}$ above the salt diapir.

10.3.7 Heat flow around fractures

Heat transport by advection commonly takes place through aquifers, but may also occur through fractures. The strength of advective or convective heat flow relative to that by conduction is measured by a Péclet number (§2.2.5). During transit through a fracture hot fluids lose heat to the rock walls, so it is a two-dimensional problem of (vertical) flow along the fracture plane and lateral heat flow into the surrounding rock (Appendix 60).

Solution of this 2D problem shows that isotherms bend upwards along the fracture and return to horizontal a lateral distance from the fracture. This lateral distance is approximately the vertical extent of the fracture l_0 (Fig. 10.8). The characteristic time for the fracture to heat up its surroundings must depend on the length of the fracture l_0, and the thermal diffusivity of the rock, $t = l_0^2/\kappa$. If the diffusivity is $10^{-6}\,m^2\,s^{-1}$, the time scale ranges from weeks to >300 years for fracture lengths l_0 of 1 m to 100 m. In geological terms, therefore, fractures heat their surroundings almost instantaneously, but the thermal effects are relatively close to the fracture. If fractures are long and closely spaced, the entire rock volume would be heated to values close to the temperature of the fluid filling the fracture (Fig. 10.8).

10.3.8 Heat flows around sills, dykes and underplates

Some basins, especially those associated with lithospheric stretching, have been intruded by igneous bodies such as dykes and sills as in the rifts of northeast Africa (Fig. 10.9). Some of these sills and dykes were emplaced at temperatures of c.1000 °C at shallow levels into rocks with temperatures in the range 0–100 °C. It is of some interest, therefore, whether the heating of dykes and sills has a significant

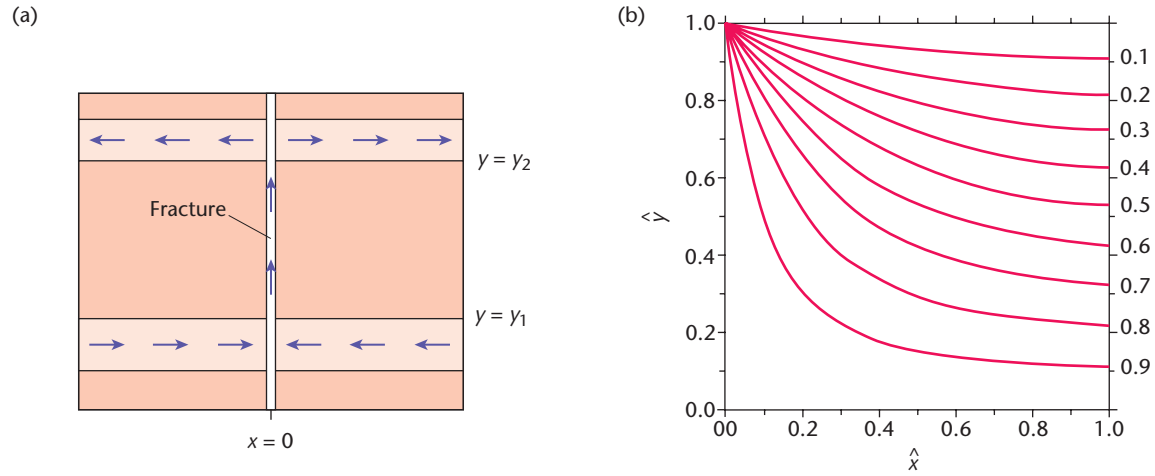

Fig. 10.8 (a) Set-up for a fracture connecting two horizontal aquifers, separated by the vertical distance y_1–y_2, with arrows showing fluid flow; (b) isotherms adjacent to a vertical fracture extending from 0 to 1 along the dimensionless vertical coordinate $\hat{y}$, where the horizontal distance is also scaled by the vertical height of the fracture l_0. Note that the isotherms swing up towards parallelism with the fracture, indicating heating from the fracture fluids, whereas at a distance of $x > l_0$, the isotherms are horizontal, indicating negligible heating from the fracture. For effective heating of the basin-fill, the fracture spacing must therefore be less than the fracture length. After Wangen (2010, figs 6.22 and 6.23). © Magnus Wangen 2010, reproduced with the permission of Cambridge University Press.

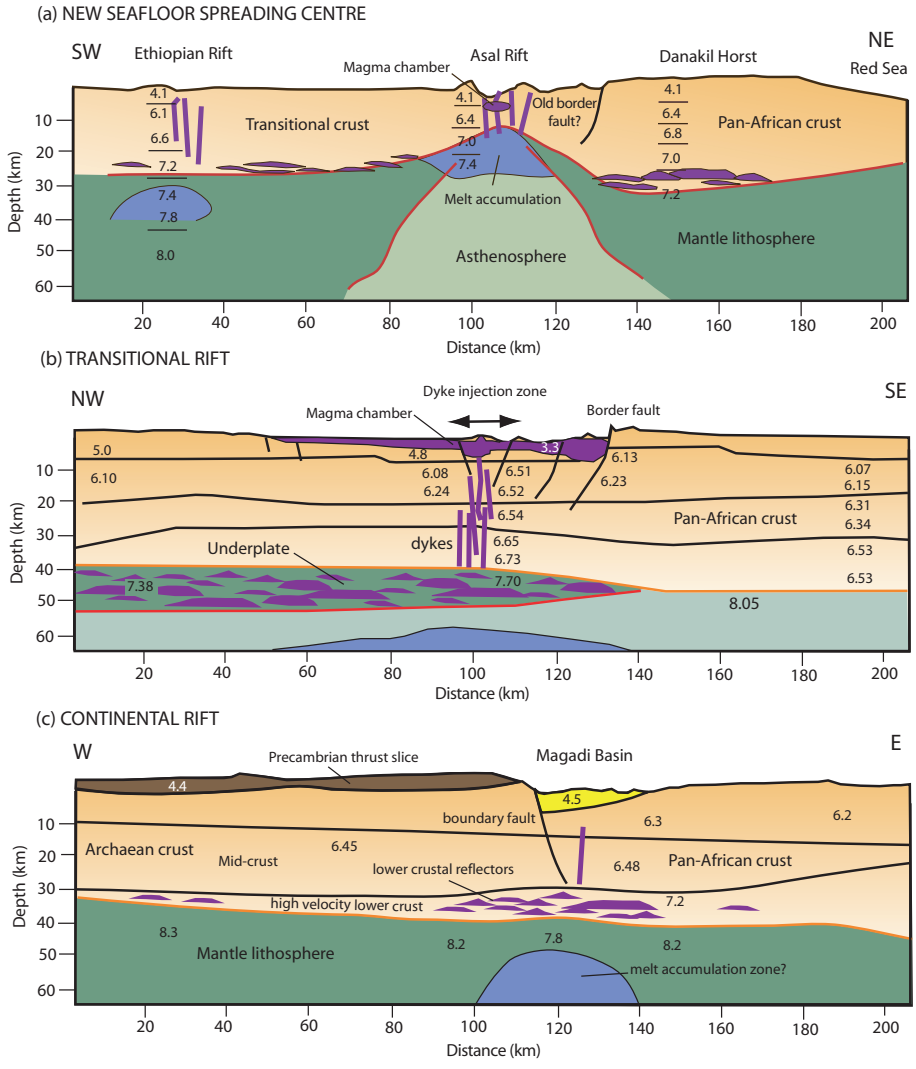

Fig. 10.9 Schematic cross-sections showing the evolutionary development from a continental rift in the south (c), through a transitional rift (b) to a new oceanic spreading centre in the north (a), in the African-Arabian rift system (after Ebinger & Scholz 2012, p. 196, fig. 9.9). Thick red line is Moho, orange is top of thick igneous underplate. Dykes sourced from the mantle and shallow magma chambers are also shown. Dyke injection takes up a considerable amount of horizontal extension and potentially has a strong impact on the thermal state of basin sediments. Numbers are seismic refraction velocities in km s^{-1}. Reproduced with permission of John Wiley & Sons, Ltd.

effect on the temperatures experienced by the sedimentary rocks of the basin-fill.

The heating of igneous bodies can be clearly demonstrated in the increase in vitrinite reflectance values in rocks adjacent to sills (Fig. 10.10). The heating is effective for a distance into the country rock or basin sediments roughly equal to the sill width, but also depends on the emplacement temperature of the sill. Consequently, very thick igneous accretions, such as underplates beneath the Moho, should have significant transient effects on the geotherm through the lithosphere and on surface heat flux (Fig. 10.11).

Let us take the example of a sill with a half-width a, an emplacement temperature of T_0, and let the sill rock and the country rock have the same thermal diffusivity κ. Let the distance from the centre of the sill be y, and let the temperature at any distance from the centre of the sill be T. If we make the temperature dimensionless by introducing $T^* = T/T_0$, the distance dimensionless by introducing $y^* = y/a$, and time dimensionless by introducing a characteristic diffusional time $t^* = t/\tau$, where $\tau = a^2/\kappa$, the temperature field can be solved in a manner similar to the cooling of ocean lithosphere, as discussed in §2.2.7.

The time taken for the sill to cool depends on its thickness, and ranges from days to thousands of years. For the country rock outside of the sill, the temperature first rises, reaches a maximum, and then falls. The dimensionless time t^*_{max} taken to reach the maximum temperature at a dimensionless distance y^* is approximated by

$$t^*_{max} \approx \frac{y^{*2}}{2} \qquad [10.14]$$

and the dimensionless temperature maximum is approximated by

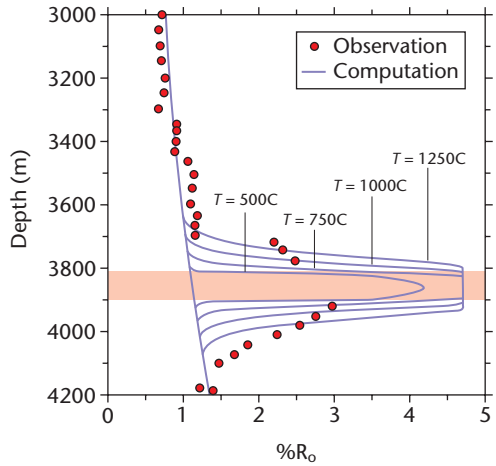

Fig. 10.10 Vitrinite reflectance observations from a borehole penetrating a 92 m-thick sill, showing the effects of heating adjacent to the sill. Vitrinite reflectances calculated based on different sill emplacement temperatures are superimposed. Comparison with measured R_o% shows a significant discrepancy, with high R_o% values a long way from the sill margin. This is most likely due to heating by convective fluids. If so,it is likely that the sill was intruded at temperatures above c.1000 °C. The vitrinite above and below the sill is altered over a distance approximately equal to the sill thickness. After Wangen (2010, fig 6.30a). © Magnus Wangen 2010, reproduced with the permission of Cambridge University Press.

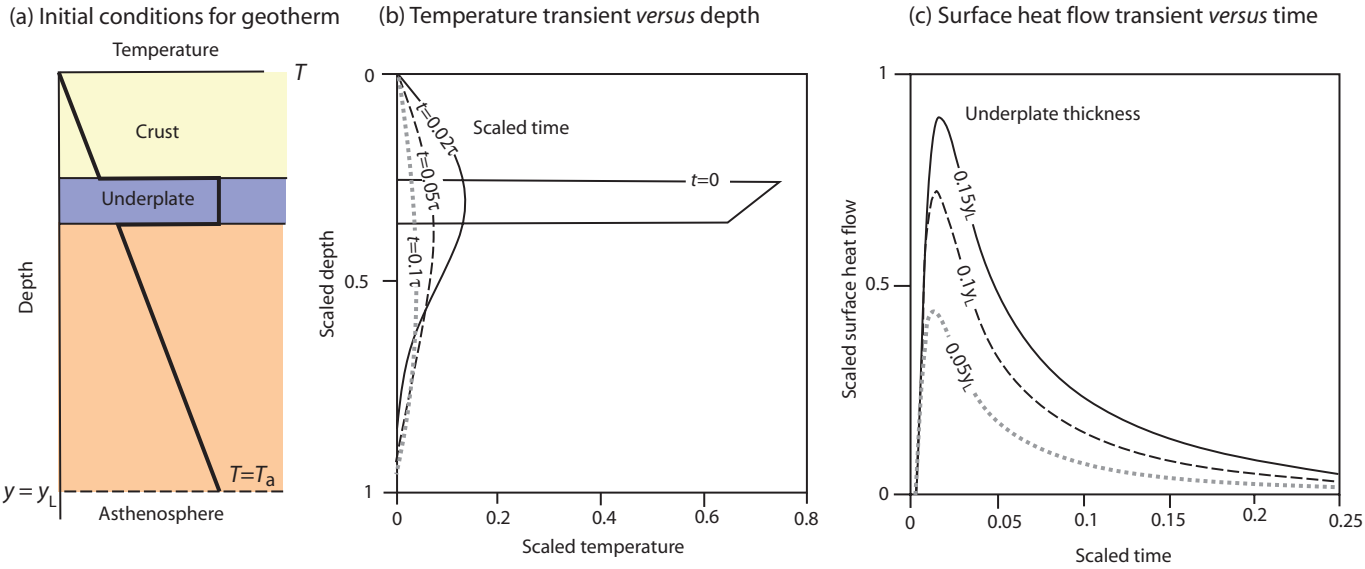

Fig. 10.11 Thermal effects of the intrusion of an igneous underplate below the Moho. (a) Initial conditions and (b) temperature profiles at different times after underplating. Temperature is normalised by the temperature at the base of the lithosphere, depth is normalised by the thickness of the lithosphere, and time by the diffusive lithospheric time constant y_L^2/κ, for an initial lithospheric thickness of 150 km. (c) Transient surface heat flux for different thicknesses of underplate. Flux is scaled by the steady-state solution prior to underplating. After Jaupart & Mareschal (2011, figs 7.18, 7.19 and 7.20). © Claude Jaupart and Jean-Claude Mareschal, reproduced with the permission of Cambridge University Press, 2002.

$$T^{*}_{max} \approx \sqrt{\frac{2}{\pi e}} \frac{1}{y^{\star}} \qquad [10.15]$$

where e is the exponential coefficient (2.73).

With increasing distance from the sill, the time of the achievement of maximum temperatures also increases, but with increasing distance the magnitude of the maximum temperature diminishes. Far from the sill at $y^{*} = y/a = 100$ (10 sill half-widths from the centre line of a 10 m-thick sill), eqn. [10.14] gives $t^{*}_{max} = 5000$, which gives a time of 16 kyr for a diffusivity of $10^{-6}\,m^2\,s^{-1}$. From eqn. [10.15] the maximum temperature impact from the sill is c.50 °C. However, close to the sill at $y^{*} = 2$ (20 m from the centreline of a 10 m-thick sill), the max temperature is achieved at a time of just 6 years. The maximum temperature impact from the sill is c.340 °C at this position.

The heating from the sill is clearly extremely important in affecting thermal maturity, but is restricted within a zone approximately one to two sill widths either side of it. As we have seen (Fig. 10.10), thermal indicators such as vitrinite reflectance and apatite fission track ages will be reset by the thermal effects of the sill within this zone.

For igneous underplates, we can assume that the initial temperature of the underplated material is the same as the temperature of the asthenosphere. As the material is molten or partially molten, its solidification will release latent heat (Jaupart & Mareschal 2011, p. 210). The solutions for the temperature field surrounding the underplate and the surface heat flow are shown graphically in Figs 10.11b and 10.11c. The temperature transient (scaled by the asthenospheric temperature) decays rapidly in amplitude over time (scaled by the diffusive time scale y_L^2/κ), and is never large except very close to the underplate.

Inserting reasonable values for the initial lithospheric thickness (y_L=125 km), thermal diffusivity (κ=$10^{-6}\,m^2\,s^{-1}$), and initial underplate temperature T_0 of 1100 °C, the temperature transient is a maximum of 165 °C 10 Myr after emplacement. But after 50 Myr, the temperature transient has reduced to a maximum of about 55 °C.

The surface heat flux peak occurs some time after underplate emplacement. For a thick underplate of thickness 18.75 km, the surface heat flux transient is nearly equal to the steady-state heat flux through the lithosphere (c.30 mW m^{-2}); it occurs 10 Myr after emplacement and decreases to close to background values after about 100 Myr.

The thermal effects cause an uplift of the overlying Earth's surface due to the effects of thermal expansion over the lithospheric thickness. The amplitude of uplift is likely to be small and depends primarily on the thickness of the underplate. If the volumetric coefficient of thermal expansion $\alpha = 3 \times 10^{-5}\,K^{-1}$, and the excess temperature of the underplate compared to the surrounding temperature is 600 °C, the surface uplift is 0.018 times the underplate thickness, that is, it is c.340 m for an underplate thickness of 18.75 km.

10.3.9 Thermal effects of delamination

Delamination, or convective removal, of the mantle lithosphere and its replacement by asthenosphere has been invoked for the surface uplift of orogenic plateaux regions such as Tibet (England & Houseman 1989; Jiménez-Munt & Platt 2006). This is expected to have effects in terms of the surface heat flow as well as uplift of the topographic surface. The effects of the thermal perturbation are shown in Fig. 10.12.

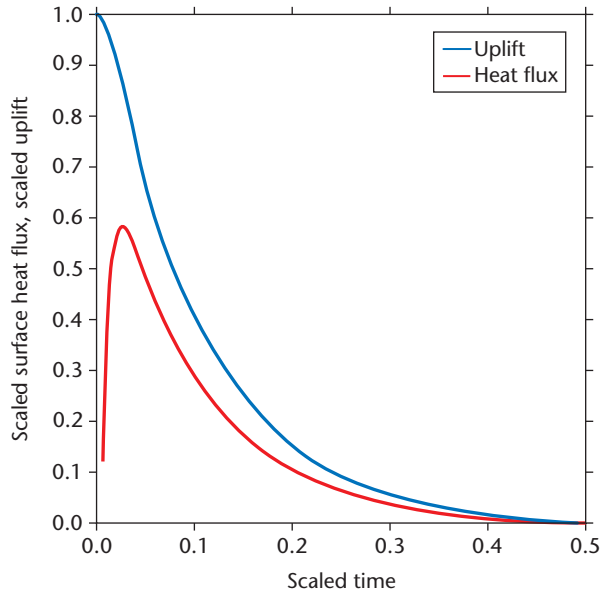

Fig. 10.12 Thermal effects of delamination. Surface flux variation (red line) and surface uplift (blue line) after delamination of the lithospheric mantle. Crustal thickness is ¼ initial lithospheric thickness. Heat flow is scaled by the steady-state solution prior to delamination, and time by the diffusive time scale of the lithosphere y_L^2/κ. After Jaupart & Mareschal (2011, fig. 7.21). © Claude Jaupart and Jean-Claude Mareschal, reproduced with the permission of Cambridge University Press, 2002.

In Fig. 10.12 the surface heat flux scaled by the steady-state heat flow prior to delamination lags behind the surface uplift by c.25 Myr and its amplitude is relatively small, consistent with the generally low surface heat flow values measured in regions such as the Colorado Plateau. For a Moho temperature of 600 °C and an initial lithospheric thickness of 150 km, the surface heat flux transient is just 7.5 mW m^{-2}, so the effect on basin thermal maturity is negligible. The surface uplift, however, instantly peaks at the time of the delamination and its amplitude is of the order of 1 km for reasonable parameter values. Delamination is therefore important in uplifting the Earth's surface but, in the absence of crustal extension, is unimportant in affecting the thermal maturity of basin sediments.

10.4 Measurements of thermal maturity in sedimentary basins

Approaches to understanding the mechanisms of subsidence and uplift in sedimentary basins invariably involve model predictions for burial history, heat flow and paleotemperature that can be compared with observational evidence. But what direct observations are possible in a sedimentary basin that provide information on thermal history and thereby allow a test and calibration of these models? A wide range of techniques are currently available, making use of the changes with temperature of organic particles, clay minerals, geochemical markers, and of the annealing and diffusion histories of certain minerals such as apatite. Most of these techniques generate data on the *maximum* temperature reached by a particle within the basin-fill. This is because thermal reactions are irreversible. Only

thermochronological techniques such as apatite fission track and U–Th/He analyses provide any information on thermal evolution. Each technique has its advantages and drawbacks. Taken together, a range of diverse techniques may provide important information on the thermal history of the basin-fill. This information is critically important, not only in understanding the driving mechanisms for basin formation, but also in the evaluation of hydrocarbon prospectivity (Tissot & Welte 1978) (chapter 11).

In the following sections, a number of techniques are presented in outline. For further information and detailed applications, the reader is referred to the references cited. Useful summaries are found in Héroux *et al.* (1979), Gallagher *et al.* (1998), Giles (1997) and Beardsmore and Cull (2001). Thermochronological techniques are covered by Braun *et al.* (2006) and in the compilation edited by Lisker *et al.* (2009).

10.4.1 Estimation of formation temperature from borehole measurements

Formation temperatures from boreholes are used in thermal modelling studies to calculate the geothermal gradient and basal heat flow of the sedimentary section. The temperature in the borehole is recorded on each logging run, using a suite of maximum recording thermometers. Because the circulation of drilling fluid tends to cool the formation, it is necessary to analyse the rate at which temperature restores itself to its original true formation value using temperatures recorded on each successive logging run within a suite of logs. These temperatures may be plotted on a 'Horner'-type plot, as described by Dowdle and Cobb (1975).

The form of the temperature build-up plot is shown in an example from the Gulf Coast in Fig. 10.13. Temperature measured on each logging run is plotted against a dimensionless time factor, $(t_c + \Delta t)/\Delta t$, where t_c is the cooling time (the duration of mud circulation from the time the rock formation opposite the thermometer was drilled to the time circulation of the drilling mud stopped), and Δt is the thermal recovery time (time since mud circulation stopped to the time the logging sonde is in position at the bottom of the borehole). A fully recovered or stabilised formation temperature T_f is obtained by extrapolation to the ordinate, where $(t_c + \Delta t)/\Delta t = 1$. Serra (1984, 1986) discusses the calculation of heat flow from borehole temperature measurements.

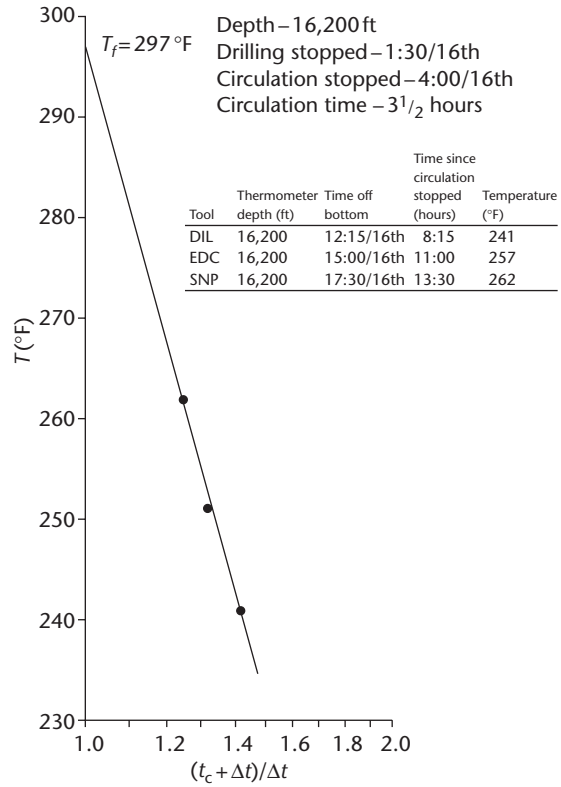

Fig. 10.13 The determination of true formation temperature from a Horner plot (after Dowdle & Cobb 1975). This example is from a high-temperature well in the Gulf Coast, USA. The depth at which measurements were taken was 16,200 ft (c.5 km). Temperature increased from 241 °F measured at 8 h 15 min after circulation of mud stopped, to 262 °F taken 13 h 30 min after circulation stopped. The estimated formation temperature T_f is 297 °F. © 1975. Reproduced with permission of Society of Petroleum Engineers (SPE).

10.4.2 Organic indicators

The progressive maturation of organic materials has long been understood in terms of *coal rank*. The coalification process changes peat to anthracite through the intermediate steps of brown coal (lignite and sub-bituminous coal) and bituminous coal. During coalification, the percentage of carbon increases whereas moisture and volatiles are gradually eliminated (Fig. 10.14). Of much greater importance to basin analysis is the quantitative measurement of maturity through the reflectance of the vitrinite maceral, and to a lesser extent the structural changes in distinctive organic molecules known as biomarkers, and the semi-quantitative assessment of spore colour.

Vitrinite reflectance is the most widely used indicator of maturity of organic materials. It is an optical parameter and is denoted by VR or R_o (reflectance in oil). Standard procedures for the measurement of vitrinite reflectance are given in Bostick and Alpern (1977), Bostick (1979), Hunt (1979), Dow and O'Connor (1982), Stach *et al.* (1982), van Gijzel (1982) and Tissot and Welte (1984). The reflectance of the vitrinite group of macerals appears to vary smoothly and predictably with temperature (Lopatin 1971; Burnham & Sweeney 1989; Sweeney & Burnham 1990).

Drawbacks in the use of vitrinite reflectance measurements are outlined by Héroux *et al.* (1979), Kübler *et al.* (1979) and Durand *et al.* (1986). These arise from a number of problems. Reflectance measurements taken from maceral types other than vitrinite (especially in lacustrine and marine sediments), and even from different macerals within the vitrinite group, may significantly differ (Bensley & Crelling 1994). Other drawbacks are the possibility of reworking of organic material (especially in sandstones), and the lack of higher plants yielding vitrinite in pre-Devonian strata. Vitrinite reflectance tends to be unreliable at low levels of thermal maturity (R_o less than 0.7 or 0.8%). At high temperatures equivalent to depths of >4 km the vitrinite maceral is increasingly anisotropic, making accurate measurement problematical. Nevertheless, with care, reflectance values are a good indicator of maximum paleotemperature within the approximate depth range of 1 to 4 km (Whelan & Thompson-Rizer 1993).

Unfortunately, the distribution of activation energies and value of the frequency factor (see eqn. [10.1]) for the maturation of vitrinite

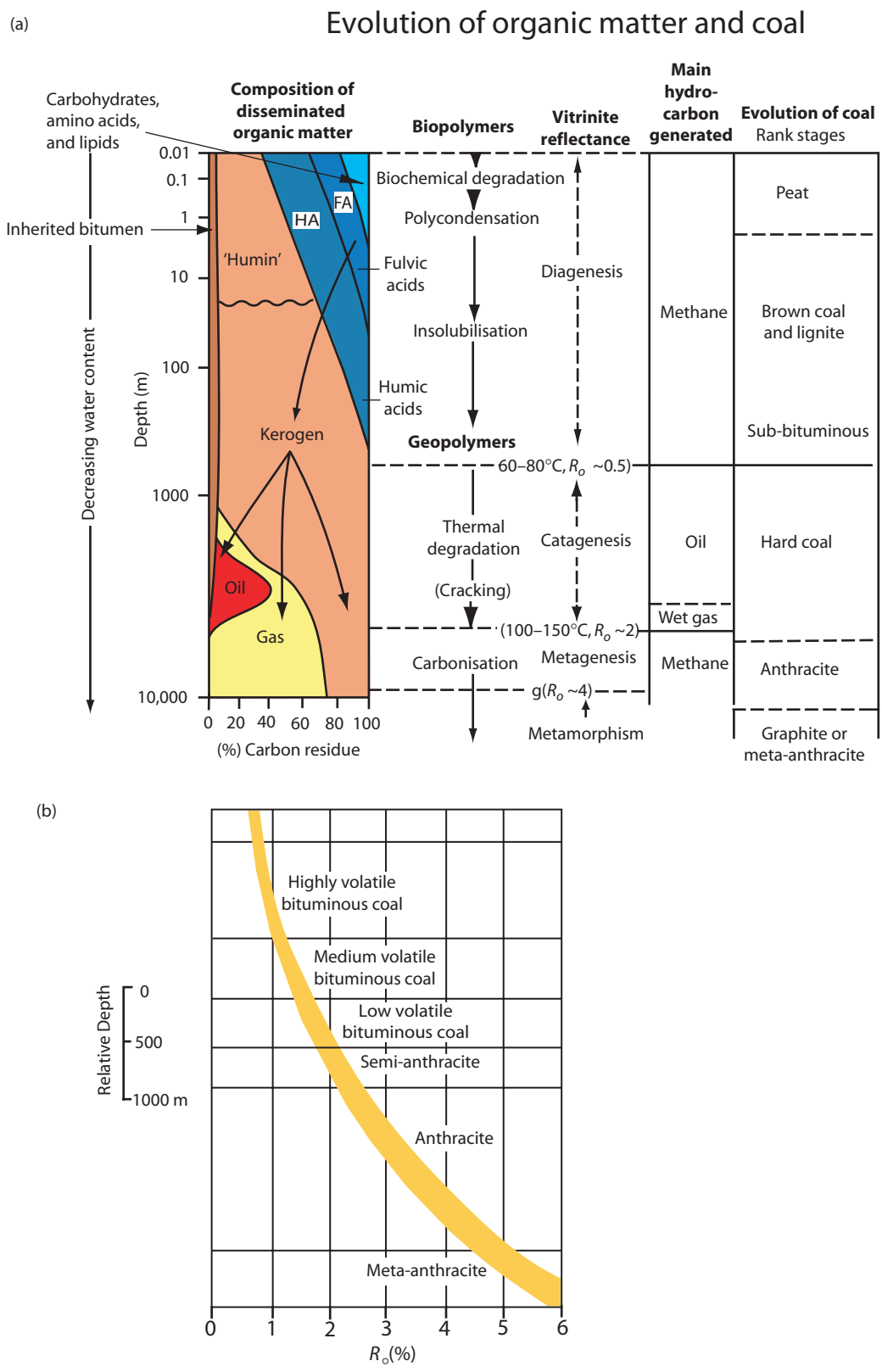

Fig. 10.14 (a) Evolution of organic matter from organic-rich sediment or peat through the various ranks of coal to meta-anthracite, and the main hydrocarbons generated, correlated with vitrinite reflectance values. After Tissot & Welte (1984), reproduced with kind permission from Springer Science+Business Media B.V. Coal ranks from Stach *et al*. (1982). (b) Correlation of coal rank with vitrinite reflectance R_0 (%).

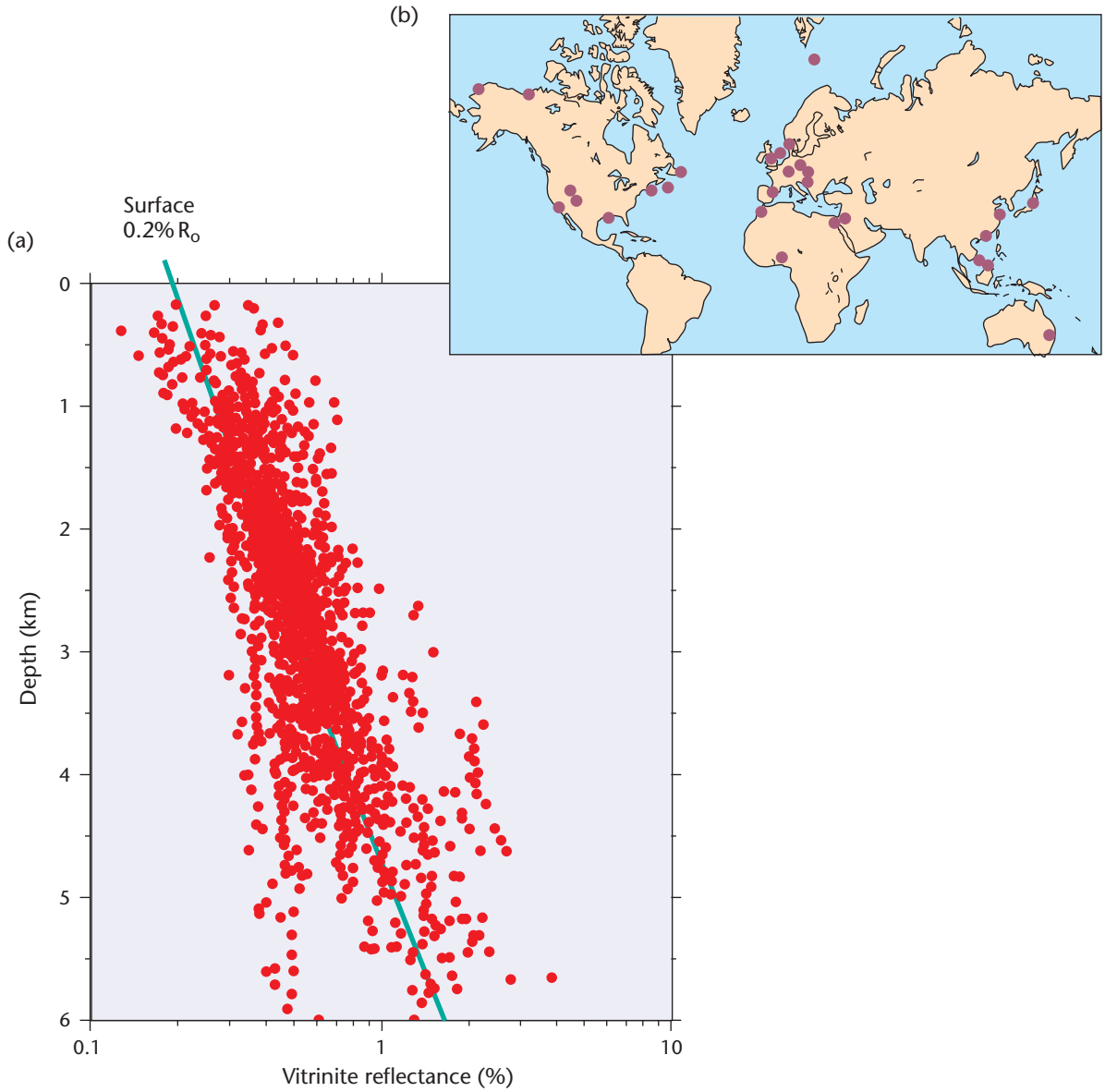

Fig. 10.15 (a) Vitrinite reflectance (logarithmic scale) versus depth for a wide range of selected extensional sedimentary basins (marked on world map in (b)) with predictable subsidence histories. After Rowley & White (pers. comm.).

are not convincingly known (Lerche *et al.* 1984; Burnham & Sweeney 1989; Lakshmanan *et al.* 1991), and a wide range of values has been proposed. The most reliable estimates give a value of E_a in the range 200–300 kJ mol^{-1}, and of A from 2.5×10^{10} to 7.48×10^{18} s^{-1}. It must be emphasised, therefore, that the uncertainties in knowledge of the parameters in the Arrhenius equation make the use of vitrinite reflectance data useful but inexact, and VR measurements should always be compared with paleotemperature estimates from other indices.

Vitrinite reflectance measurements from samples recovered at different depths allow a plot of vitrinite reflectance versus depth to be made (e.g. Corcoran & Clayton 2001). These plots are known as VR or R_o profiles. Examples of their interpretation are given in §10.5.1. A compilation of VR data from 28 extensional basins shows a relatively well-defined trend (Fig. 10.15), with a surface intercept at 0.2 to 0.4% R_o, and a gradient of $0.15 \pm 0.09\%$ R_o km^{-1} at depths of <4 km.

The Anadarko Basin in western Oklahoma has some of the deepest exploratory wells in the world, penetrating to more than 7900 m (~26,000 ft), and is therefore an excellent case study for thermal maturation. Vitrinite reflectance contours (*isoreflectance lines*) on the Upper Devonian–Lower Mississippian *Woodford Shale* have been constructed from 28 boreholes (Fig. 10.16) (Cardott & Lambert 1985). Isoreflectance maps are useful in combination with structural contours, since cross-cutting relationships give an indication of local thermal anomalies superimposed on the burial-related maturation.

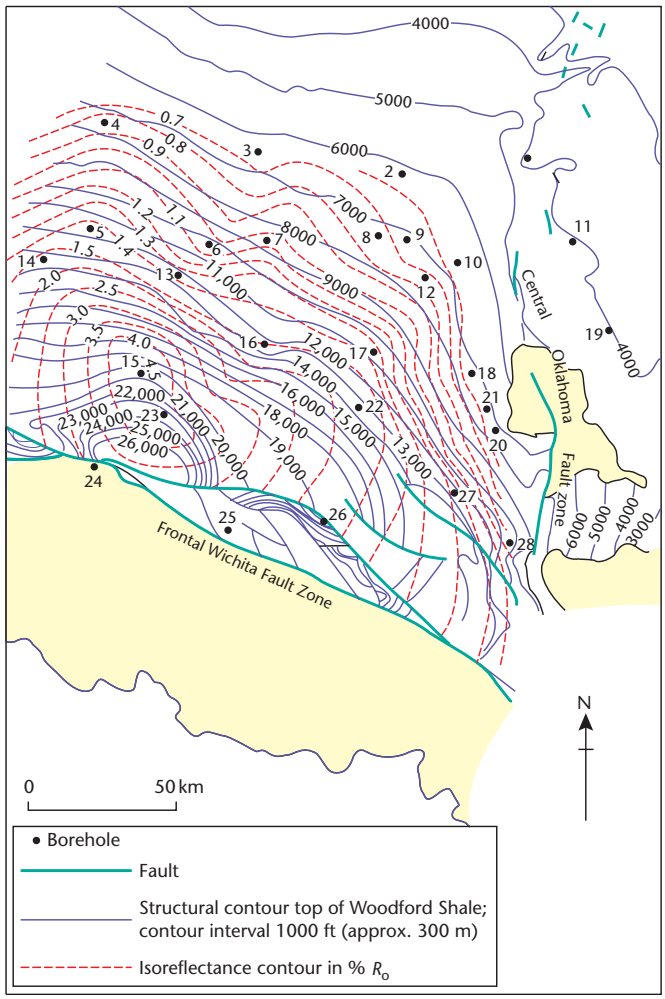

Fig. 10.16 Combined isoreflectance and structure map of the Woodford Shale of the Anadarko Basin of Oklahoma (Cardott & Lambert 1985). Vitrinite reflectance values in general increase with depth of burial, but strong cross-cutting relationships of the isoreflectance and structure contours suggest that there may have been local thermal disturbances superimposed on the burial-related maturation. AAPG © 1985. Reprinted by permission of the AAPG whose permission is required for further use.

Since vitrinite reflectance is a non-reversible thermal indicator, it is important to know whether the distribution of vitrinite reflectance with depth in a sedimentary basin allows a geotherm at a particular time in basin history to be constructed. For example, is it possible that the maximum temperature at different depths in the basin was reached at different times? If so, a R_o profile would not represent a single geotherm that existed at a particular time. This problem can be approached from a forward model of paleotemperature and vitrinite reflectance in a basin with a time-dependent basal heat flow. The heat flow and temperature algorithms are based on the uniform stretching model, but with an additional heat flow originating from the internal heat generation of crustal rocks and sediments due to radioactive decay. The time-temperature history of a number of horizons within a model borehole can then be calculated based on the thermal model and the subsidence history derived from the stratigraphy penetrated by the borehole. Paleotemperatures can be converted to vitrinite reflectance using empirical relationships (Barker & Pawliewicz 1986; Burnham & Sweeney 1989; Sweeney & Burnham 1990) to create a synthetic VR profile (Fig. 10.17).

Two interacting effects control the paleotemperature and vitrinite reflectance of the stratigraphy filling stretched basins. On the one hand, the basal heat flux decreases through time due to thermal relaxation following stretching, causing cooling. On the other hand, subsidence causes a reference horizon to descend to increasing depths over time, causing heating. Fig. 10.17 shows that for low to moderate values of stretching in a basin undergoing continuous subsidence, the present-day temperatures represent the maximum temperatures reached by all but the deepest horizons within the basin-fill. Consequently, the vitrinite reflectance profile can be used to estimate the geotherm. However, model results suggest that in highly stretched basins and for old (especially syn-rift) stratigraphy, VR values may represent maximum paleotemperatures attained early in basin history and not subsequently exceeded. Consequently, measured VR profiles may not accurately reflect the distribution of temperature with depth at any particular instant in time.

The use of R_o profiles in estimating the amount of section removed as a result of basin inversion events is discussed in §10.5.1.

Although vitrinite reflectance has become pre-eminent in its use in basin studies, it is not the only index of thermal maturity. Other optical parameters derived from organic material include sporinite microspectrofluorescence and spore, pollen and conodont colouration scales. Fluorescence and reflectance studies are complementary, fluorescence intensity and reflectance being inversely proportional.

Certain organic molecules (*biomarkers*) undergo transformations with increasing temperature. For example, single *isomers* in biological material are progressively converted to mixtures of isomers with increasing temperature (Abbott *et al.* 1990). *Aromatisation* reactions can also be used, such as the conversion of mono-aromatic to tri-aromatic steroids (Mackenzie & McKenzie 1983). Biomarker transformations take place at rates approximated by the Arrhenius equation.

10.4.3 Low-temperature thermochronometers

Low-temperature thermochronometers are discussed in relation to estimates of erosion in §7.3. The emphasis in this section is on the use of low-temperature thermochronometers in assessing the thermal history of the basin-fill.

Fission track analysis is a very widely used thermochronological technique based on the atomic damage caused to minerals such as apatite, zircon and sphene by their spontaneous decay, almost exclusively by the fission of ^{238}U. The fission of ^{238}U produces a trail of damage to the lattice, known as a *fission track*. Fission tracks become visible when the crystal is chemically etched and viewed at high magnification.

Fission track ages and track length distributions differ according to the time-temperature history of the mineral. For example, *linear heating* (Fig. 10.18a), which may be thought of as characteristic of the trajectory of deposited detrital apatite grains followed by burial in the basin-fill, produces a tightly clustered, unimodal, symmetrical histogram of track length with a short mean track length (MTL). All tracks experience the same maximum temperature. The fission track age bears no relation to any specific or thermal event. Alternatively, basin inversion may cause *heating followed by cooling* (Fig. 10.18b). Old tracks formed during the heating phase have a similar length, with a short MTL. Newer tracks experience different maximum

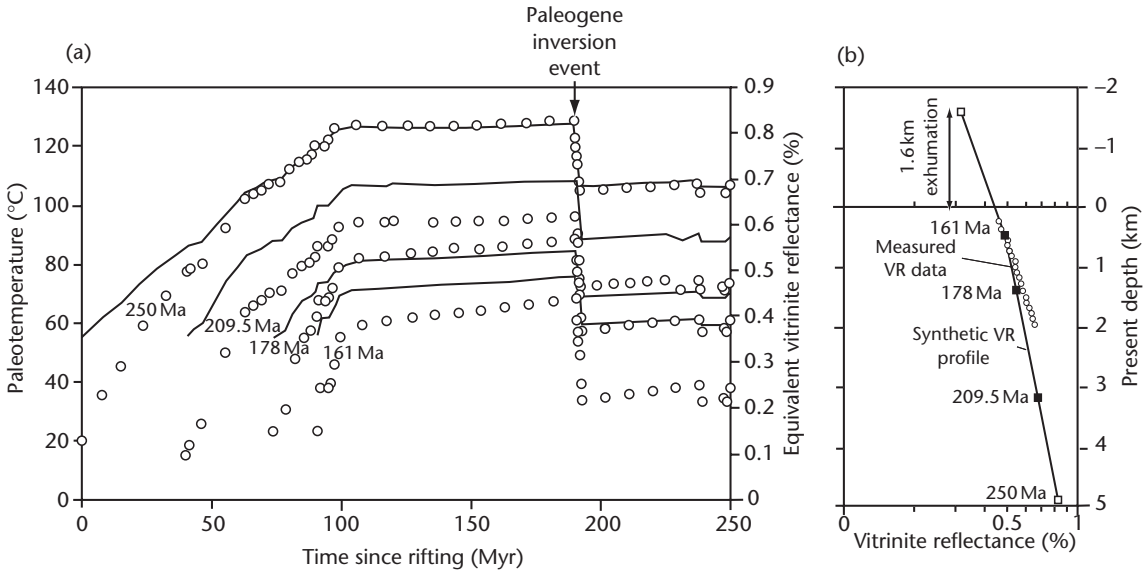

Fig. 10.17 (a) Paleotemperature and equivalent vitrinite reflectance versus time for four different horizons in well 42/21-1 in the extensional Irish Sea Basin ($\beta = 1.5$ at 250 Ma) with internal heat generation ($H_s = 9.6 \times 10^{-10}$ W kg^{-1}; $h_r = 10$ km) and the thermal conductivity structure shown in Fig. 10.2. Open circles are data points derived by forward modelling temperature from the borehole subsidence history. Solid lines are equivalent vitrinite reflectance. (b) The forward modelled R_0 profile is compared with measured values. Extrapolation of the profile upwards gives an estimate of 1.6 km of denudation since the VR values were set at the maximum temperature at c.60 Ma (c.190 Myr since rifting).

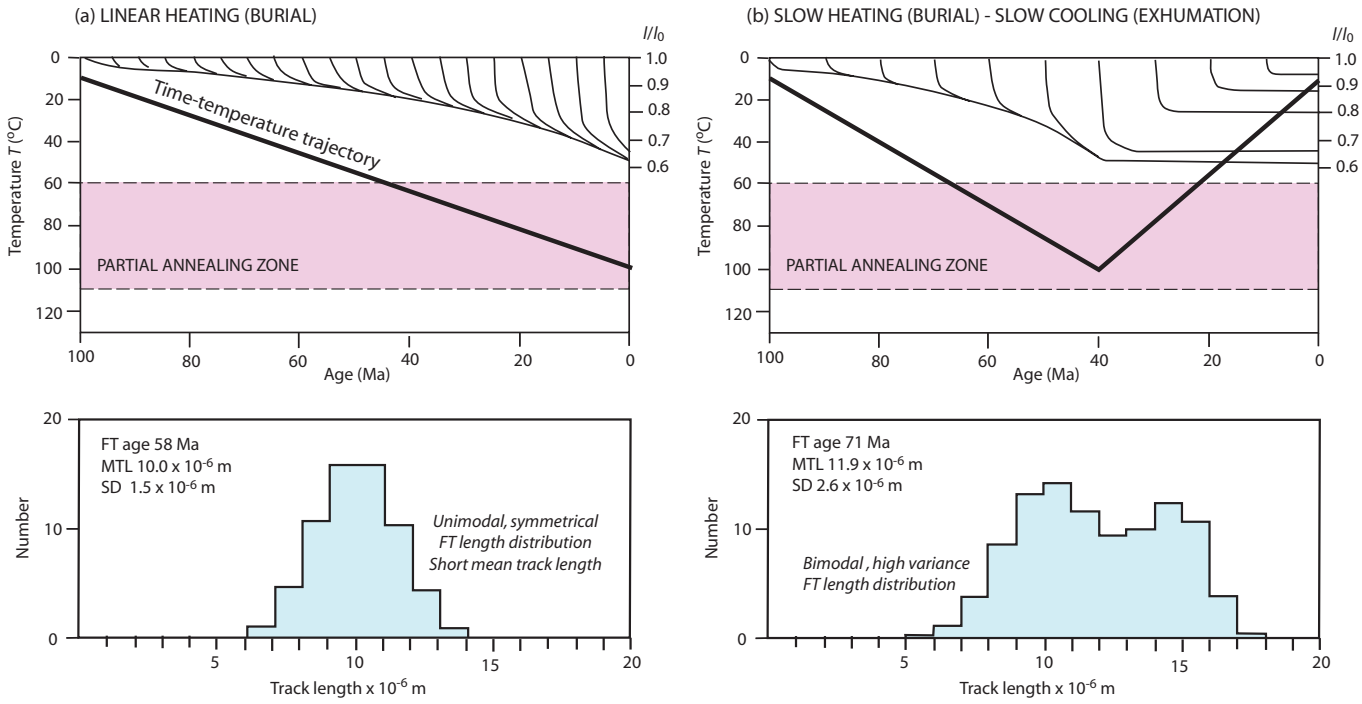

Fig. 10.18 Simple thermal histories and the predicted fission track length parameters using Durango apatite and the annealing model of Laslett *et al*. (1987), after Gallagher *et al*. (1998). Each model simulation has 20 tracks formed at equal-time increments over the total duration of the thermal history. Track length reduction (annealing) is shown by the ratio l/l_0, where l is the track length and l_0 is the initial track length. Heavy solid line is time-temperature trajectory. MTL, mean track length. (a) Linear heating as a result of burial, giving a unimodal and symmetrical track length histogram with a short mean track length of 10×10^{-6} m and a standard deviation of 1.5×10^{-6} m. The fission track age (58 Ma) does not correspond to any distinct tectonic or thermal event; (b) Heating-cooling, due to slow burial and slow exhumation, causes a bimodal track length distribution with a mean track length of 11.9×10^{-6} m and a large standard deviation of 2.6×10^{-6} m. The fission track age (71 Ma) does not correspond to any distinct tectonic or thermal event.

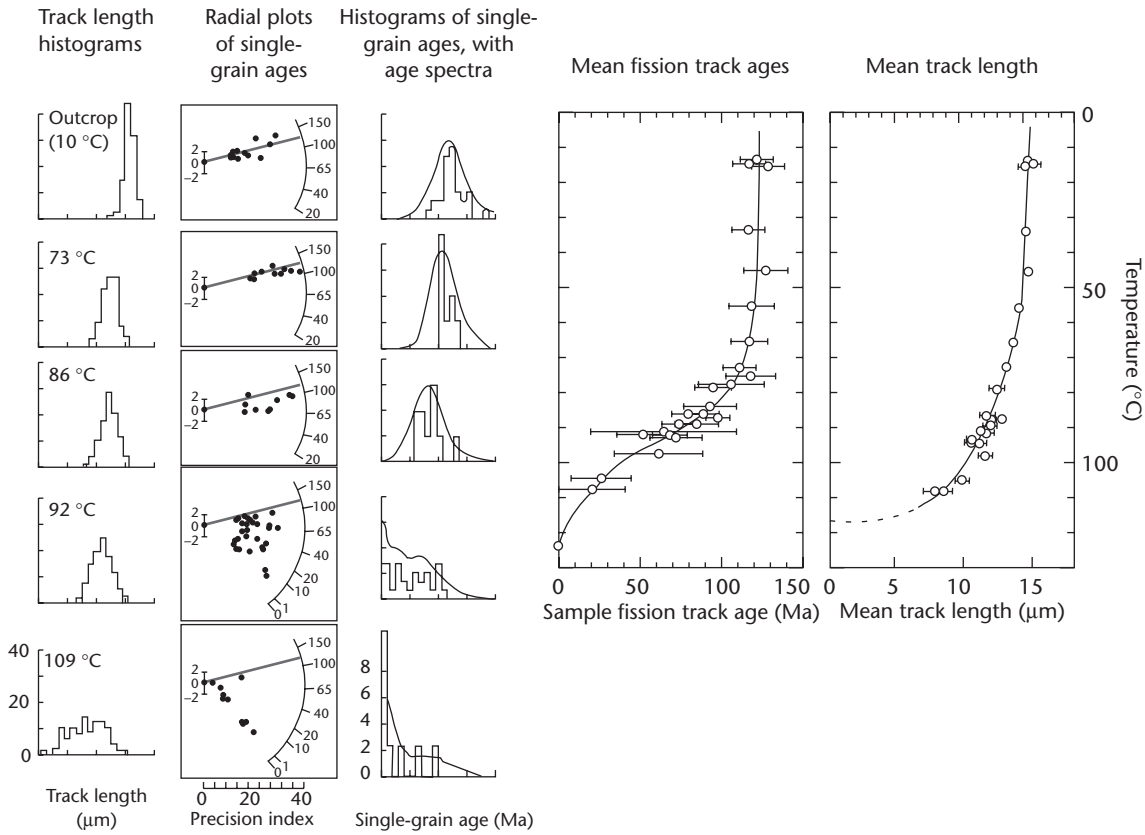

Fig. 10.19 Apatite fission track data from the Otway Basin, southeast Australia (Gleadow & Duddy 1981). The stratigraphic age of the samples is c.120 Ma (shown on the radial plots as a grey band). Note the progressive annealing of fission tracks and reduction of fission track ages of single grains with depth of burial. Reprinted with permission from Elsevier.

temperatures during the cooling phase, causing the histogram to be bimodal, with a high standard deviation. The fission track age does not accurately reflect the timing of the onset of basin inversion.

Apatite fission track analysis has been extensively applied to the thermal history of sedimentary basins (Naeser 1979). This is because the temperature range over which apatite fission track analysis is sensitive (c.50 °C to 120 °C) is also the temperature range over which hydrocarbons are generated (Gleadow *et al.* 1983). The fission track data from the Otway Basin of Australia (Gleadow & Duddy 1981) illustrate the important principles (Fig. 10.19). At shallow depths above the partial annealing zone (PAZ), the fission track lengths are tightly clustered and long (c.14 μm), indicating minimal annealing. The fission track age is more or less equivalent to the stratigraphic age of the samples (120 Ma). With greater depth, fission track length histograms show a wider distribution and a shorter MTL. The fission track ages decrease due to the greater amount of annealing at elevated temperatures, reaching 0 Ma at a temperature of 120 °C (Fig. 10.19).

Detrital grains commonly contain a combination of information on their exhumational history in the source area and their burial history in the basin (Rohrman *et al.* 1996; Carter & Gallagher 2004). Apatite fission track analysis of a number of samples at different depths in a sedimentary basin can be used to calculate geothermal gradients if the effects of the exhumational history can be identified (§10.5.2).

The U–Th/He method is used less in basin studies because the thermal history is reset at relatively low temperatures (50–70 °C) that are common in sedimentary basins. Helium age distributions are known to decrease rapidly down boreholes because of the effect of temperature on diffusion rates (Wolf *et al.* 1998).

There are a number of factors that may affect the distribution of temperature with depth, including variations in thermal conductivity, effects of fluids and internal heat generation. Consequently, calculation of geothermal gradients from apatite fission track data alone are likely to be significantly in error. A combination of paleothermal data from apatite fission track, vitrinite reflectance and any other available techniques is therefore always advised.

10.4.4 Mineralogical and geochemical indices

Mineralogical parameters are controlled by the temperature and chemical properties of the diagenetic environment of the sediment (Fig. 10.20). A number of diagenetic models exist (e.g. Frey *et al.* 1980; Burley *et al.* 1985; Worden & Morad 2003) that allow an interpretation of the sequence of authigenic minerals in terms of their relationship to their depositional environment or surface chemistry (*eogenesis*), the burial or subsurface conditions (*mesogenesis*), and the weathering or re-exposure to surface conditions (*telogenesis*).

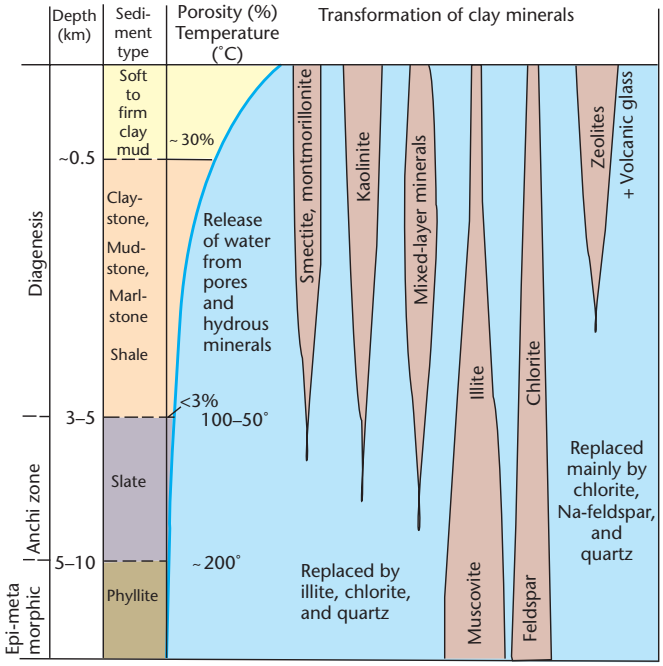

Fig. 10.20 Mineralogical indices. Diagenesis of clay-rich sediments as a function of depth and temperature, showing the most important mineral transformations. After Frey *et al.* (1980); Heling (1988).

The reader is referred to §11.5 for further details on the impact of diagenesis on carbonate and sandstone reservoirs.

Since eogenetic changes are strongly related to depositional environment, climate and associated pore water chemistry, they are of limited use in thermal modelling. However, mesogenesis marks the removal of the sediment from the predominant influence of surface agents in the interstitial pore water. A number of temperature-dependent reactions commonly take place in siliciclastic rocks. Kaolinite transforms to dickite, smectites transform to illite via a process of interlayering, and chloritisation takes place. Physical processes accompany these chemical changes during burial diagenesis. The most important result is *compaction* due to the weight of the overlying sediments (§9.2). In sandstones, compaction brings about a number of porosity-reducing adjustments, including initial mechanical compaction, which simply compresses grains together, rotation, grain slippage, brittle grain deformation and fracturing and plastic deformation of ductile grains.

The best-documented mineral transformations of use in evaluating thermal maturity are from shaly mudstones, where the clay mineral assemblages, the position of the (001) reflection of smectite, the percentage of illite layers in the mixed-layer illite 2:1 expandable, and the illite crystallinity index are used. Derivation of an approximate relationship between mineralogical changes of this type and organic maturity indices has been attempted (Fig. 10.21). One of the fundamental problems is the need for quantitative indices with which to correlate temperature-driven changes. Kübler *et al.* (1979), for example, proposed a quantitative measure of the crystallinity of illite using the width of the illite peak on an X-ray diffractogram measured at half of the peak height. The beginning of oil generation (R_o = 0.5%) has been correlated with the disappearance of smectite (e.g. Powell *et al.* 1978; Kübler *et al.* 1979).

Quartz cementation and consequent porosity loss is also a temperature-related process acting in sandstones buried to temperatures above 60 °C (Walderhaug 1996). It is dealt with in more detail in §10.5.3. At about the same temperature of 60 °C, smectite clay starts to react with K-feldspar to form illite (Hower *et al.* 1976; Nadeau & Reynolds 1981). At higher temperatures of 100–120 °C, illite precipitates at the expense of kaolinite and K-feldspar (Bjorlykke *et al.* 1986). This can be seen in the percentage of illite in the clay fraction of sandstones penetrated by wells on the Norwegian continental shelf (Fig. 10.22). Quartz cementation and illite precipitation are both temperature-dependent, with activation energies of c.15 kcal mol^{-1} and 20 kcal mol^{-1} respectively. The combined temperature-driven effects of quartz cementation and illite precipitation makes sandstones that have experienced temperatures above 120 °C unattractive as potential reservoirs and aquifers (§11.5).

The K content of diagenetic illites allows the age of illite growth to be calculated using the ^{40}K–^{40}Ar radiometric technique. K–Ar ages from samples obtained from different depths can then be used to plot age-depth relationships (Hamilton *et al.* 1989). The K–Ar age should, for a continuously subsiding basin, increase with depth, since the deeper horizons should reach the critical temperature for illite cementation first. A study of sandstone reservoir rocks from the Brent province of the North Sea showed that illite growth began at temperatures of 100–110 °C (corresponding to a vitrinite reflectance in overlying shales of 0.62%), but that there was considerable scatter in the K–Ar age/depth relationship (Hamilton *et al.* 1992).

The investigation of inclusions of fluids in the rocks and minerals of sedimentary basins forms part of a broader field of paleofluid analysis (Parnell 2010). The inclusions are microscopic bubbles of fluid (or gas) trapped within crystals or fractures. The inclusions preserve their composition and pressure-temperature conditions at the time of entrapment (Fig. 10.23). The fluids analysed commonly come from quartz cements (Walderhaug 1994) and microfractures in quartz grains (Parnell *et al.* 2005). In petroliferous basins, the paleofluids may be hydrocarbons.

The passage of hot fluids through a sedimentary basin is marked by fluid inclusion temperatures far in excess of those expected from the geothermal gradient. In many cases these elevated temperatures must be due to transport of hot fluids up faults and through aquifers (Ziagos & Blackwell 1986; Hulen *et al.* 1994). These high temperatures may represent inversions of the normal temperature profile in the sedimentary basin. Fluid inclusions also allow transient thermal events to be recorded, which are not recorded in other thermochronometers that are based on a time integral for maturity, such as vitrinite reflectance.

10.5 Application of thermal maturity measurements

10.5.1 Vitrinite reflectance (R_o) profiles

Vitrinite reflectance measurements can be plotted as a function of depth to give R_o profiles. The slope of the R_o curves gives an indication of the geothermal gradients in the history of the basin. Although

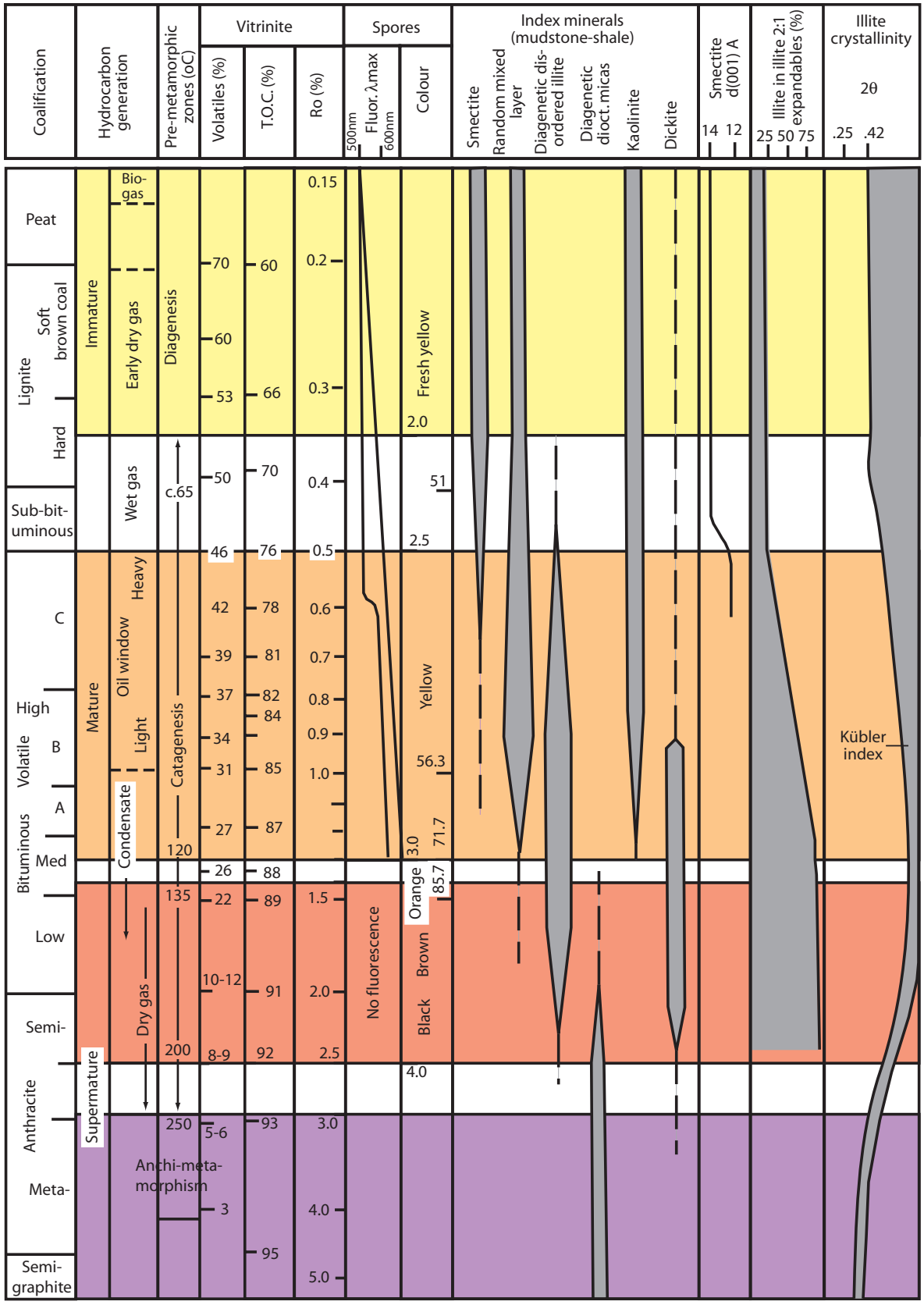

Fig. 10.21 Comparison of a range of thermal indices, modified from Héroux *et al*. (1979). Thermal indices shown are coal rank, vitrinite total organic carbon and % volatiles, vitrinite reflectance, spore fluorescence and colouration, typical clay mineral distributions, position of the (001) reflection of smectite, percent illite in the mixed layer illite 2:1 expandable, and illite crystallinity (Kübler index). These indices are correlated with temperature and hydrocarbon products generated. AAPG © 1979. Reprinted by permission of the AAPG whose permission is required for further use.

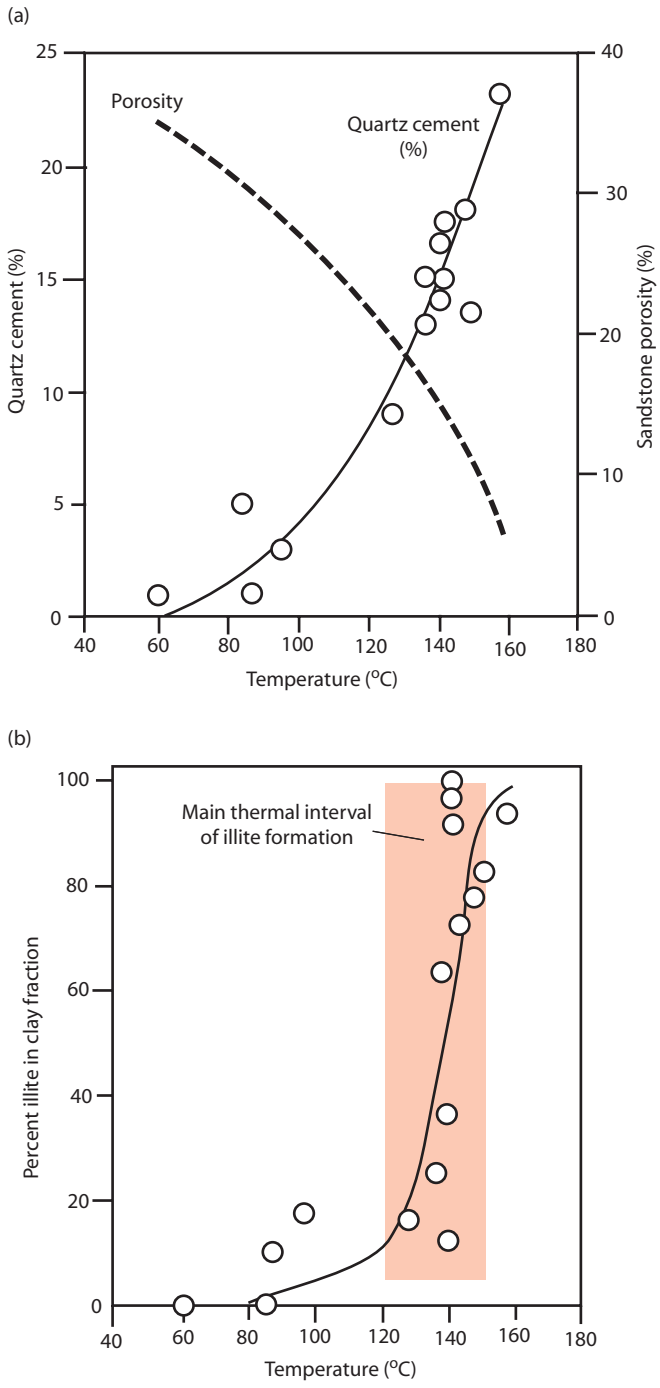

Fig. 10.22 (a) Plot of temperature versus quartz cement content and porosity for wells from the Norwegian continental shelf (Bjorkum & Nadeau 1998), showing an exponential increase in amount of quartz cement with depth. (b) Plot of temperature versus diagenetic illite content measured by X-ray diffraction. Increasing illite content severely reduces permeability. The main thermal interval for illite formation is 120–150 °C.

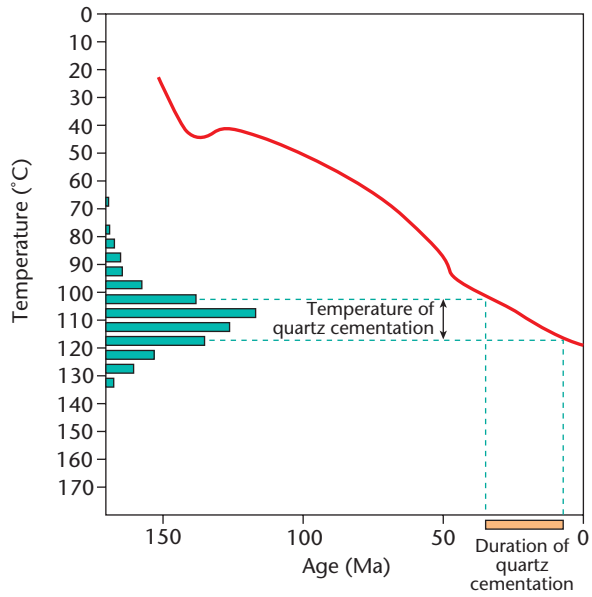

Fig. 10.23 Timing of quartz cementation derived from the combination of temperatures of cementation from fluid inclusion analysis (green bars) with paleotemperature from burial history (red line), Upper Jurassic Brae Formation of Miller Field, northern North Sea. Line shows temperature history of the uppermost part of the Brae Formation in well 16/7b-20 based on a burial history analysis. The temperature range of quartz cementation is based on fluid inclusion analysis of authigenic quartz cements. Quartz cementation took place 35–10 Myr ago. From Gluyas *et al*. (2000), reproduced with permission of John Wiley & Sons, Ltd.

many profile shapes are possible (Fig. 10.24), they generally indicate an exponential evolution of the organic matter with time (Dow 1977), as expected from the kinetics described in §10.2. In basins largely unaffected by major unconformities, young dip-slip faulting and localised igneous activity, there should therefore be a linear relationship between depth and log R_o. Plots of large numbers of reflectance measurements from many sedimentary basins worldwide (Fig. 10.15) (Rowley & White 1998), or from many locations within a basin system (Corcoran & Clayton 2001), show a strong clustering along a roughly linear trend in depth-log R_o space, with an intercept at a depth of zero of 0.2 to 0.4% (Fig. 10.15).

Individual R_o profiles follow a number of different trends, each of which is diagnostic of a particular thermal history. An example of a simple sublinear profile is the Terrebonne Parish well in Louisiana (Heling & Teichmüller 1974) (Fig. 10.24a). R_o is 0.5% at 3 km and 1% at 5 km. It indicates a normal and constant geothermal gradient through time. The Woodford Shale of the Anadarko Basin is another example of a sublinear R_o profile with a surface intercept at $R_o = 0.2\%$, indicating the amount of maturation that the vitrinite had undergone prior to deposition (Fig. 10.24b).

Other R_o profiles are more complex. A dogleg pattern of two linear segments of different slope indicates that two periods of different geothermal gradient have occurred. This may result from a thermal 'event' occurring at the time presented by the break in slope. Such an interpretation is plausible for the R_o profiles from boreholes in the Rhine Graben (Teichmüller 1970, 1982; Robert 1988) (Fig. 10.25).

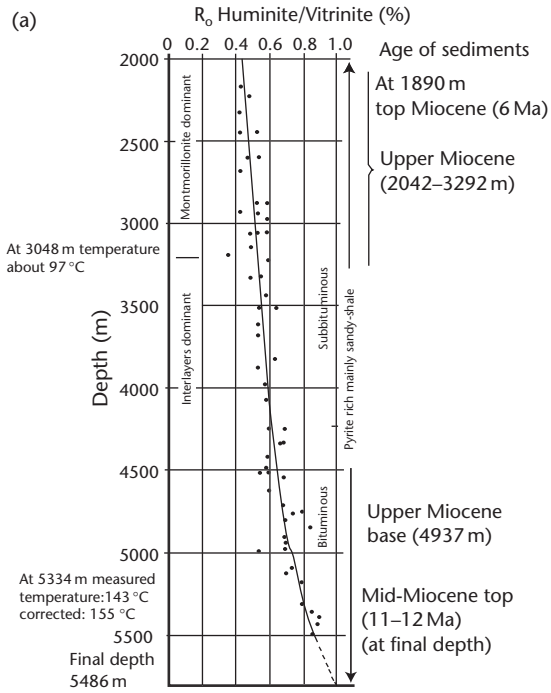

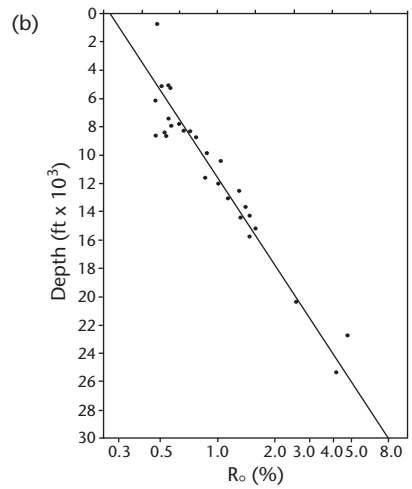

Fig. 10.24 (a) Vitrinite reflectance profile for Terrebonne Parish, Pont au Fer well in Louisiana. The profile is sublinear and continuous, suggesting a near-constant geothermal gradient through time (after Heling & Teichmüller 1974; reproduced with permission from Springer Science+Business Media B.V.). (b) Woodford Shale of the Anadarko Basin also shows a good sub-linear trend (Cardott & Lambert 1985; AAPG © 1985, reprinted by permission of the AAPG whose permission is required for further use).

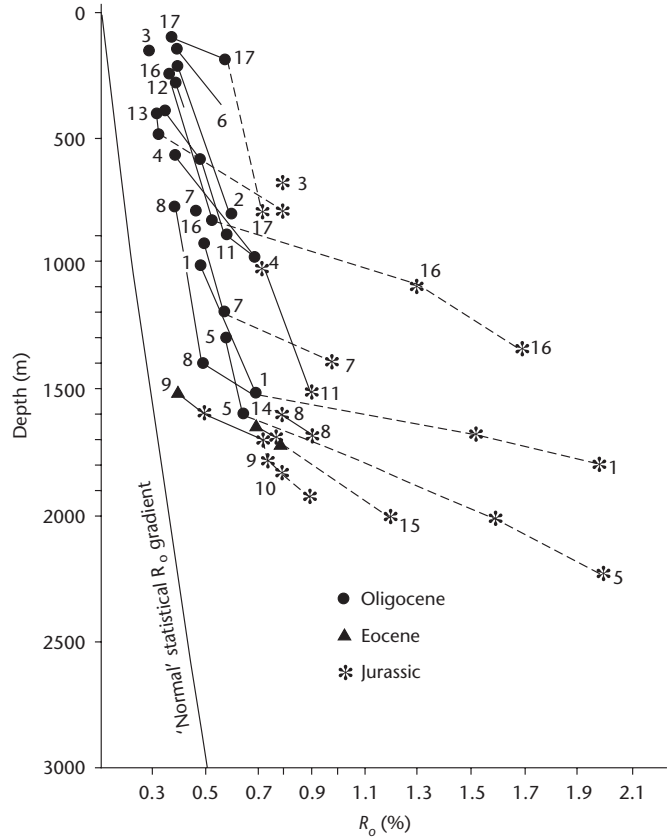

1 Scheibenhard 101–2
2 Croettwiller 1
3 Reimerswiller 1
4 Schaffhouse 3
5 Roeschwoog 1
6 Donau 2
7 Haguenau 2
8 Gambsheim 1
9 Kilstett 1
10 Holsheim 1
11 Eschau 1-11
12 Meistratzheim 1
13 Schaeffersheim 1
14 Colmar South 1
15 Blodesheim 1
16 Galfingue 1
17 Knoeringue1

Fig. 10.25 Reflectance profiles from a number of wells in the Alsace region of the Rhine Graben (after Teichmüller 1970). In general, there are pronounced dog-legs in the R_o profiles at about the age of the Oligocene–Eocene boundary. The post-Eocene history shows a 'normal' gradient, whereas the pre-Oligocene sedimentary rocks have high reflectance values in relation to their depth of burial. This suggests that rifting in the late Eocene caused higher than normal maturity in the older rocks of the basin-fill. Reproduced with kind permission from Springer Science+Business Media B.V.

R_o profiles may consist of two sublinear segments offset by a sharp break or jump in R_o values. The jump may correspond to an unconformity with a large stratigraphic gap. This is well illustrated in the Mazères 2 borehole in the Lacq area of the Aquitaine Basin, France (Fig. 10.26), where R_o values jump from c.0.8% to c.2.4% at the level of an unconformity separating Aptian–Albian rocks from underlying Kimmeridgian.

If there is a known (logarithmic) relationship of R_o with depth, and the subsidence history of a sedimentary basin is known, the R_o values give an indication of the variation of the geothermal gradient through time. This then allows different tectonic histories to be tested (Middleton 1982).

10.5.1.1 Estimation of structural inversion from R_o profiles

R_o profiles can be used to estimate the amount of denudation resulting from a period of basin inversion, since the vitrinite locks in information about the maximum paleotemperature experienced. The technique has been used extensively, particularly in the region of the northwest European continental shelf surrounding the British Isles, where an important crustal uplift event took place in the Early Tertiary (Rowley & White 1998). This uplift event, which was

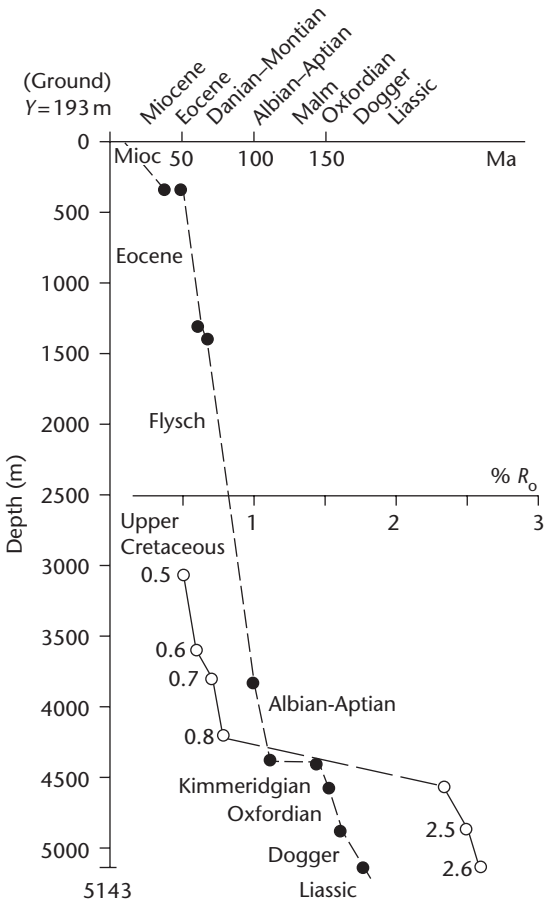

Fig. 10.26 Vitrinite reflectance profile for the Mazères borehole in the Lacq region of southern France (open circles, with reflectance value), and depths of stratigraphic units (black circles). The sharp increase in R_o marks an unconformity between the Lower Cretaceous and the Upper Jurassic. After Robert (1988), reproduced with kind permission of Springer Science+Business B.V.

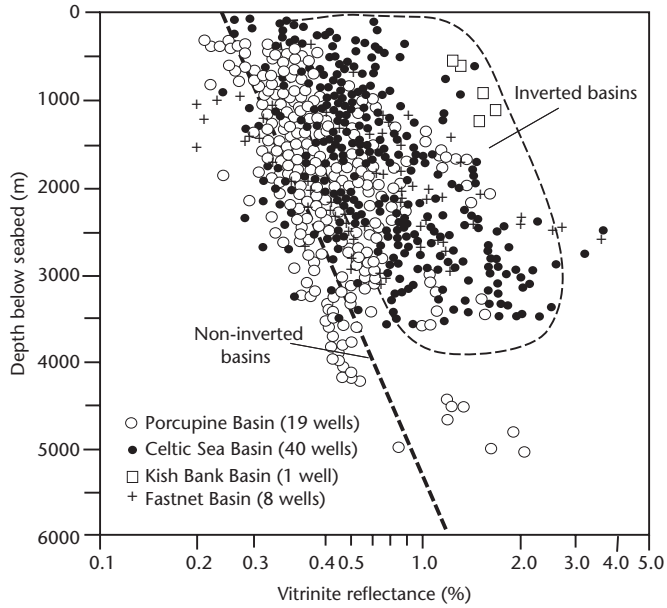

Fig. 10.27 Vitrinite reflectance versus depth for Mesozoic and Cenozoic successions penetrated in boreholes in a number of basins offshore Ireland (Corcoran & Clayton 2001). Basins such as the Porcupine Basin show a 'normal' R_o profile indicative of continual subsidence, whereas those basins that have experienced tectonic uplift and exhumation (such as the Celtic Sea, Kish Bank and Fastnet basins) have displaced R_o profiles indicating higher thermal maturity than expected from the present depth of burial.

most likely related to the thermal, isostatic and dynamic effects of the Icelandic plume (White 1988; Brodie & White 1994) caused an unconformity that cuts down variably into Mesozoic rocks in the form of a paleo-river drainage system (Hartley *et al.* 2011). The paleotemperature profiles from areas such as the Irish Sea basin system are linear and sub-parallel to the present-day geotherm (Duncan *et al.* 1998), suggesting that heating was caused primarily by burial rather than by basal heat flow variations or local magmatic and fluid flow effects. However, most of the R_o values in boreholes in the British-Irish area have elevated values compared to the global data set of non-inverted basins (Fig. 10.27) (Corcoran & Clayton 2001). Calculations of the amount of denudation from the R_o profile can be performed using a number of different methods:

- The curve of log R_o versus depth is extrapolated linearly upwards to a value of approximately 0.2% R_o (Dow 1977; Corcoran & Clayton 2001). The displacement of the depth axis is the amount of denudation. Although this method has been very widely applied, it makes the erroneous assumption that the geothermal gradient is linear. This is a particularly poor assumption in the shallow parts of basins where thermal conductivities vary strongly. It is more likely that the geotherm is convex near the surface. Secondly, large errors may result from the incorrect choice of surface temperature (and therefore R_o at $y = 0$) at the time of maximum paleotemperatures.
- Maximum depths of burial can be estimated from VR values from empirical relations such as (Barker & Pawlewicz 1986).

$$\ln(R_o) = 0.00096T - 1.4 \qquad [10.16]$$

  where T is the temperature, which must be converted to depth using a geothermal gradient. The empirically derived depth can be compared with the present-day depth of the sample. However, there are large uncertainties in the accuracy of the R_o-T relationship.
- Vitrinite reflectance can be calculated from a forward thermal model using the kinetic approaches described in §10.2 (e.g. Middleton 1982). A comparison of observed VR values with the results of a number of forward models allows the most likely parameter values and amount of denudation to be estimated. Alternatively, the amount of denudation can be estimated by inverse methods using the same chemical kinetics.
- Amounts of inversion can be estimated from the trends in sonic velocity versus depth (Giles 1997; Giles & Indrelid 1998; Ware & Turner 2002). For a given lithology, such as shales, the curve between sonic interval transit time and depth reflects the maximum depth (or minimum porosity) attained by a given interval. Inverted successions have smaller porosities and faster sonic velocities than found in continuously buried successions.

Increasingly, vitrinite reflectance data are interpreted alongside other thermal indicators, such as apatite fission track thermochronometry. Both techniques require a conversion between depth and

temperature. It is estimated that total fission track annealing in apatites (closure temperature) with typical chlorine content corresponds to a vitrinite reflectance value of 0.7%. This in turn corresponds to a temperature of 110–120 °C.

10.5.2 Fission track age-depth relationships

We saw above that low-temperature thermochronometers such as apatite fission track and U–Th/He are liable to be fully or partially reset during burial in sedimentary basins (Rohrman *et al.* 1996; Carter & Gallagher 2004). Potentially, the source-area fission track signal can be separated from the burial fission track signal by the inversion of track length distributions.

Samples taken as continuously as possible along a stratigraphic depth transect (such as a borehole) are plotted in terms of apatite central age and the peak age of the youngest subpopulation. An example is given from the Miocene–Pliocene Siwalik Group exposed in the Karnali River of western Nepal (Fig. 10.28). Superimposed on the age-depth chart is the depositional age of the samples (Gautam & Fujiwara 2000). Samples at shallow levels of <2500 m depth have increasing AFT ages and youngest subpopulation ages with depth, and are older than the stratigraphic age. These samples are not annealed and record a thermal history of source-area denudational cooling. They have a lag time of ~2 Myr, indicating rapid exhumation of apatites from the Himalayan mountain belt. At depths greater than 2500 m, however, AFT central ages and youngest subpopulation ages decrease down-section, and are younger than the stratigraphic age. These samples have been partially annealed by the elevated temperatures experienced during burial in the foreland basin. The onset of annealing marks the top of the fossil apatite partial annealing zone (PAZ), representing temperatures of ~60 °C. Since this occurs at a stratigraphic depth of about 2500 m, the geothermal gradient in the basin is c.20 °C km^{-1} if surface temperature is assumed to be 10 °C. The thermochronological data do not give the geotherm deeper in the sedimentary basin since the base of the PAZ, below which detrital samples should be fully annealed and have a constant fission track age with depth, is not found in the Nepalese samples. Where recognised, the depth of the paleo-PAZ, or partial retention zone for He, would provide an additional constraint of geothermal gradient deeper in the basin.

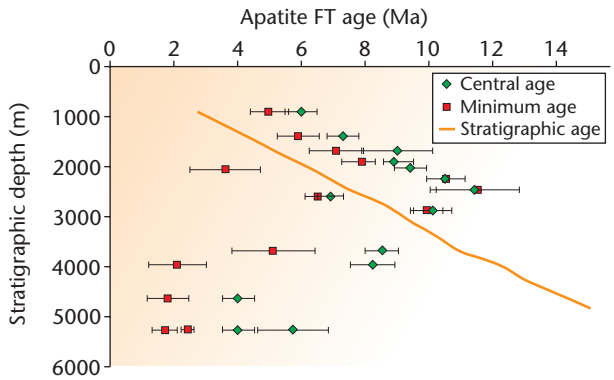

Fig. 10.28 Variations of detrital apatite fission track central age (green diamonds) and the age of the peak of the youngest component in the fission track age histogram ('minimum peak age') (red squares) with stratigraphic depth along the Karnali River section through Miocene–Pliocene (16–5 Ma) foreland basin sediment of the Siwalik Group, western Nepal (after Gautam & Fujiwara 2000). Solid line is stratigraphic age. In the upper part of the section (<2000 m), corresponding to the last 6 Myr, the minimum peak age increases down-section, and there is a nearly constant time lag of ~2 Myr between the stratigraphic age and the minimum apatite fission track (AFT) age, indicating rapid exhumation, transport and burial without annealing since deposition. Using a realistic geothermal gradient, this gives a maximum exhumation rate in the source region of about 1.5 mm yr^{-1}. Below a depth of 2000 m, peak minimum ages decrease down-section and are younger than the stratigraphic age, indicating that these samples have been annealed during burial. The transition from unannealed to partially annealed fission tracks indicates the position of the top of the paleo-partial annealing zone (PAZ), with a temperature of c.60 °C. The base of the paleo-PAZ is at the transition from partially annealed to fully annealed fission tracks. Fully annealed samples should have a constant minimum peak age with depth, with the age marking the age of final exhumation. In the lowest three samples, peak minimum ages are constant at about 2 Ma, suggesting that 2 Myr ago the Siwaliks succession was uplifted along the Main Frontal Thrust of the Himalayas. After Braun *et al.* (2006, p. 149, fig. 9.10). © Jean Braun, Peter van der Beek, Geoffrey Batt 2006, published by University of Cambridge Press.

10.5.3 Quartz cementation

Knowledge of the thermal history of a sedimentary basin enables important changes to the basin-fill to be understood and predicted, such as the occurrence of quartz cementation of sandstones (Fig. 10.23). Strongly cemented sandstones in the subsurface have little pore space left, making them unsuitable as reservoirs and aquifers (§11.5.3).

One suggestion for quartz cementation is that supersaturated pore fluids flow long distances through sandstones and locally precipitate cements, but the high number of pore volumes required makes this unlikely. Instead, dissolution-precipitation models involve: (i) the local derivation of silica by solution, and its local precipitation in adjacent pores. Dissolution takes place in a fluid film at the high stress contact points between two or more grains; and (ii) dissolution in pressure solution seams (*stylolites*) where silica solubility is enhanced by the presence of clay minerals and micas, and precipitation in interstylolite regions. Petrographic studies suggest the second dissolution-precipitation model is the more likely.

The porosity change over time in a sandstone is dependent on the reaction rate, which can be treated as an Arrhenius process, and the surface area available for quartz cementation, which is a function of porosity. For conditions where the temperature does not change with time, the porosity reduces over time to a minimum level where the pores are unconnected, known as the *percolation threshold*. The time scale over which porosity is lost depends on the specific surface (the surface area per bulk volume) available for precipitation, and the temperature. Quartz cementation is known to occur at temperatures in the range 90–120 °C. Laboratory experiments suggest that for a gravel with particles of diameter 1 cm, the specific surface is ~10^2 m^2 m^{-3}. The characteristic time for cementation is 100 Myr at a temperature of 100 °C at this value of specific surface, 75 Myr for a specific surface of 10^3 m^2 m^{-3} (equivalent to a grain diameter of 1 mm) and 50 Myr for a specific surface of 10^4 m^2 m^{-3} (finer sands) at the same temperature. These rates of cementation are faster than those calculated with Arrhenius-type kinetics (Walderhaug 1996), but the characteristic time is still very long: at 100 °C, and specific surface of 10^4 m^2 m^{-3}, typical of reservoir sandstones, pore space remains for 100 Myr.

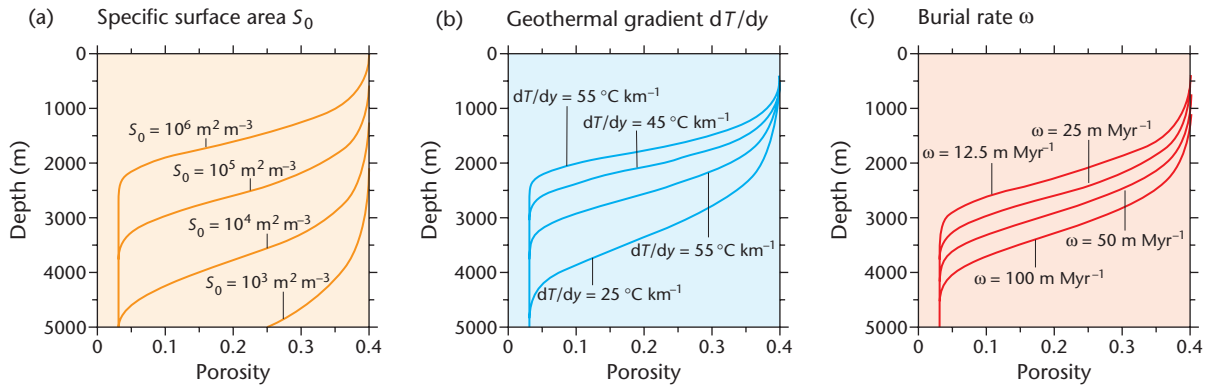

Fig. 10.29 Porosity-depth curve assuming quartz cementation during a constant burial rate (Wangen 2010, figs 11.6 and 11.7). Porosity reduction takes place by cementation only. The porosity curve depends on the initial specific surface S_0 (a), the geothermal gradient dT/dy (b) and the deposition (burial) rate ω (c). For a sandstone with specific surface area (surface area per bulk volume) $S_0 = 10^4\,m^2\,m^{-3}$, cementation starts at 2500 m and is complete by 4500 m. At a higher geothermal gradient, most of the porosity is lost by a depth of 2500 m. The impact of high temperatures is greatest at low burial rates. © Magnus Wangen 2010, reproduced with the permission of Cambridge University Press.

A constant temperature for 100 Myr is unlikely. If there were a constant rate of burial, during which time temperature increased, the quartz cementation could be married with the burial history. Neglecting the effects of compaction and assuming a constant geothermal gradient as well as a constant burial rate, the porosity-depth trajectory for a range of sandstone specific areas is shown in Fig. 10.29. The onset and termination of quartz cementation is clearly seen – from 2500 m to 4500 m for a sandstone with a specific surface of $10^4\,m^2\,m^{-3}$. In reality, compaction of the sandstone would take place before quartz cementation starts, after which cementation would retard further mechanical compaction, and further loss of porosity would be due to progressive quartz cementation. This model with constant burial rate and geothermal gradient can be modified to include a number of periods of different burial rate and geothermal gradient. For example, a period of inversion, causing cooling, would slow the cement precipitation rate, though porosity would continue to be lost (Wangen 2010, p. 375).

10.6 Geothermal and paleogeothermal signatures of basin types

We have previously seen that vitrinite reflectance measurements and apatite fission track and (U–Th)/He analysis can be used to constrain paleotemperatures and paleogeothermal gradients. Particular thermal histories are diagnostic of the formative mechanism of the basin. Robert (1988) suggested three main types of paleogeothermal history:

1 Basins with normal or near-normal paleogeothermal history

Old passive margins have present-day geothermal gradients of c.25–30 °C km^{-1} (Congo 27 °C km^{-1}; Gabon 25 °C km^{-1}; Gulf Coast, USA, 25 °C km^{-1}). The Terrebonne Parish well (Fig. 10.24a) shows a vitrinite reflectance of about 0.5% at a depth of 3 km, and the shape of the curve is sublinear. Mature passive margins therefore have near-normal geothermal gradients.

2 Cooler than normal (*hypothermal*) basins

Hypothermal basins include oceanic trenches, outer forearc and foreland basins. Ocean trenches are cold, with surface heat flows often less than 1 HFU (42 mW m^{-2}). In the Japanese archipelago Eocene–Miocene coals occur in two regions, one in Hokkaido in the north along a branch of the present-day Japan trench, and the other in Kyushu in the south is situated in a volcanic arc position relative to the Ryukyu trench. The Hokkaido region is cold, with poorly evolved coals (sub-bituminous coals with $R_o = 0.5\%$ still occurring at a depth of 5 km), whereas the volcanic arc in Kyushu is hot, containing anthracites (>2% R_o). The Mariana Trench, which is a southward continuation of the Japan trench, and its forearc region are also cold, with surface heat flows of less than 1 HFU (42 mW m^{-2}).

Foreland basins are also characterised by low present-day geothermal gradients, 22 °C km^{-1} to 24 °C km^{-1} being typical of the North Alpine Foreland Basin in southern Germany (Teichmüller & Teichmüller 1975, Jacob & Kuckelhorn 1977). The Anzing 3 well near Munich penetrates the autochthonous Molasse, undisturbed by Alpine tectonic events. At the base of the Tertiary at 2630 m depth the R_o is still only 0.51%. The Miesbach 1 well cuts through about 2 km of thrust sheets of the frontal thrust zone of the Alps (the subalpine zone), before penetrating the autochthonous sediments to a depth of 5738 m (Fig. 10.30). Even at this great depth, the R_o is still only 0.6%, indicating an abnormally low geothermal gradient during the Tertiary. The greater subsidence rate at Miesbach 1 (nearly 0.3 mm yr^{-1}) compared to Anzing 1 (0.1 mm yr^{-1}) may have been responsible for the very low geothermal gradient in the former. In summary, the low present-day geothermal gradients (Anzing 3, 22.8 °C km^{-1}; Miesbach 1, 23.5 °C km^{-1}) may have been even lower in the past during the phase of rapid subsidence related to continental collision and flexure.

3 Hotter than normal (*hyperthermal*) basins

Hyperthermal basins are found in regions of lithospheric extension such as backarc basins, oceanic and continental rift systems, some strike-slip basins and the internal arcs of zones of B-type subduction. This follows from the mechanics of basin formation in stretched

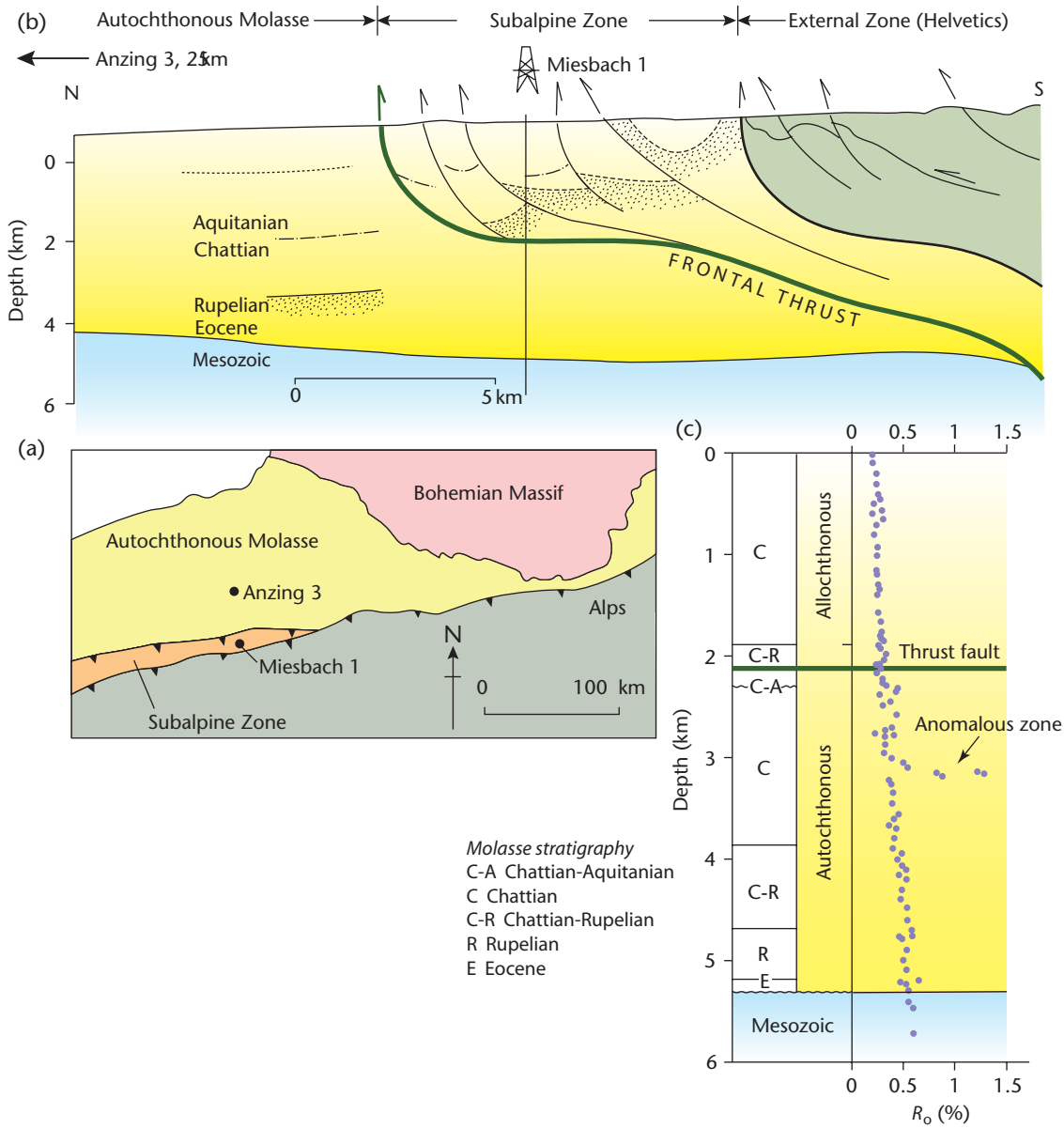

Fig. 10.30 (a) Location of the Bavarian part of the North Alpine Foreland Basin in southern Germany. Anzing 3, near Munich, and Miesbach 1, are boreholes discussed in the text. (b) Cross-section of the southernmost part of the Bavarian section of the North Alpine Foreland Basin, showing the location of Miesbach 1 in the tectonically imbricated subalpine zone (after Teichmüller & Teichmülller 1975, published with kind permission from Springer Science+Business Media B.V.). (c) The R_o profile at Miesbach 1 (Jacob & Kuckelhorn 1977) shows that the autochthonous 'Molasse' under the basal subalpine thrust is poorly evolved, not exceeding 0.6%, even at 5738 m depth. This is indicative of a very low geothermal gradient during the period of rapid sedimentation in the Oligocene.

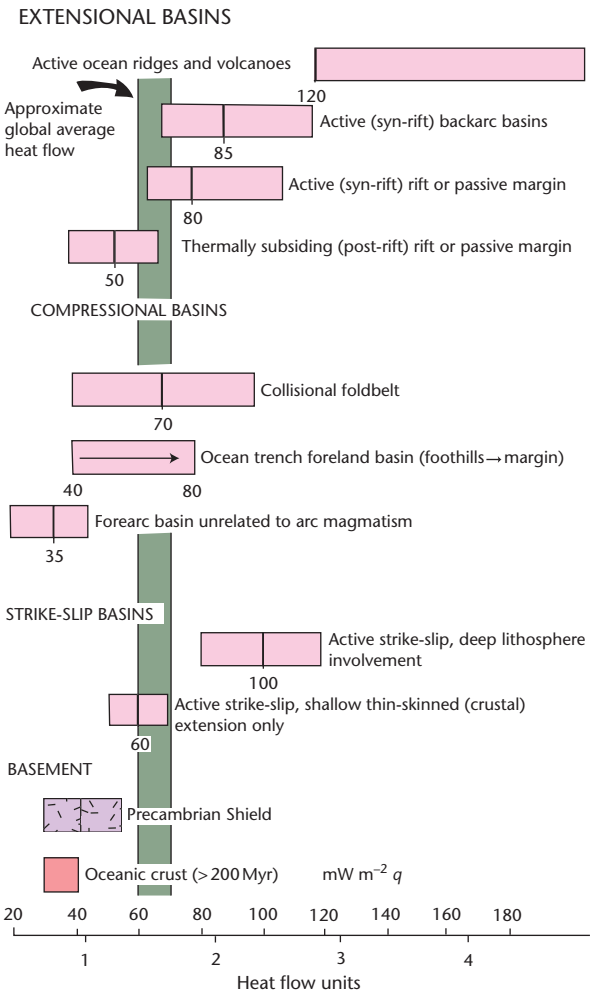

Fig. 10.31 Summary of the typical heat flows associated with sedimentary basins of various types.

regions, involving the raising towards the surface of isotherms. *Oceanic rifts* are zones of very high heat flows, 3 to 4 HFU (120–170 mW m^{-2}) being typical, and values occasionally reach 5 to 6 HFU (200–250 mW m^{-2}). Some Californian *strike-slip basins* have very high geothermal gradients (c.200 °C km^{-1} in Imperial Valley), so that very young sediments can be highly mature. Continental rifts have high present-day geothermal gradients (>50 °C km^{-1} in the Red Sea, up to 100 °C km^{-1} in the Upper Rhine Valley) and ancient continental rifts have intense organic maturations in their contained sediments.

Oceanic measurements and deep boreholes in the *Red Sea* (Girdler 1970) suggest that high surface heat flows (generally >3 HFU, >125 mW m^{-2}) occur in a broad band at least 300 km wide, centred on the axis of the rift. The organic maturation shown by R_o profiles and the occurrence of oil, gas and condensate fields suggests that the highest maturity is found in the south of the Red Sea, intermediate values are found in the north of the Red Sea, and the lowest occur in the Gulf of Suez. This can be correlated with different amounts of extension, the largest amount being in the south of the Suez-Red Sea system. The former elevated heat flows in the Oligo–Miocene of the Gulf of Suez have now diminished to near-normal values, while the southern Red Sea, which is still actively rifting, still has very high heat flows.

There are many other examples of high organic maturation in ancient continental rift basins: 2–3% R_o in the Lower Cretaceous of the Congo; 3.3% R_o in the Upper Cretaceous of Cameroon; 3.5% R_o in the Coniacian of the Benue Trough, Nigeria; and 5% R_o in the Permian of the Cooper Basin, Australia.

Internal arc heat flows are elevated because of magmatic activity. The Tertiary anthracites of Honshu, Japan (see above) (2–3% R_o) are an example. Similar patterns are found in ocean–continental collision zones such as the Andean Cordillera, and hyperthermal events may also affect parts of continent–continent collision zones such as the Alps: the 'Black Earths' of southeastern France have R_o values of over 4%, but the precise origin of the thermal event is unknown (Robert 1988, p. 261).

The surface heat flows of the main genetic classes of sedimentary basin are summarised in Fig. 10.31.